Geomorphology 423 (2023) 108548

Contents lists available at ScienceDirect

Geomorphology

journal homepage: www.journals.elsevier.com/geomorphology

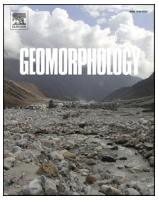

Last Glacial Maximum glacier fluctuations on the northern Alpine foreland: Geomorphological and chronological reconstructions from the Rhine and Reuss glacier systems

Sarah Kamleitner [a,*], Susan Ivy-Ochs [a], Lucia Manatschal [b], Naki Akçar [c], Marcus Christl [a], Christof Vockenhuber [a], Irka Hajdas [a], Hans-Arno Synal [a]

[a] Laboratory of Ion Beam Physics, ETH Zurich, Zurich, Switzerland
[b] Department of Earth Sciences, ETH Zurich, Zurich, Switzerland
[c] Institute of Geological Sciences, University of Bern, Bern, Switzerland

ARTICLE INFO

Keywords:
Last Glacial Maximum
European Alps
Glacial geomorphology
Cosmogenic nuclide surface exposure dating

ABSTRACT

Fresh glacial landforms of the Alpine forelands evidence the presence and extent of large piedmont glaciers during the Last Glacial Maximum (LGM) and yield valuable insights into LGM glacier dynamics. This study assesses widespread ice marginal landforms preserved within the limit of the former LGM Rhine glacier and the eastern lobes of the LGM Reuss glacier system by means of geomorphological mapping. Timing of formation of the studied ice margins in Rhine and Reuss systems are chronologically framed by new ^{10}Be and ^{36}Cl surface exposure ages, as well as new radiocarbon dates. This includes redating of radiocarbon samples first determined in the 1980s. Results of this and an earlier study focussing on outwash deposits downstream of the outer LGM ice margin, suggest that the Rhine glacier advanced to and reached its LGM maximum between ca. 26–22 ka, thereby forming a broad >100 km wide foreland piedmont lobe and constructing prominent and largely continuous chains of frontal moraines (outer Schaffhausen moraines). The eastern lobes of the Reuss glacier likely advanced to their LGM maximum position by 25/24 ± 2 ka as indicated by published luminescence dates. Stabilization of the corresponding Untertannwald ice margin and the slightly internal yet more prominent Mellingen moraines (Reuss glacier system) occurred no later than 22 ± 1 ka and 21 ± 1 ka, respectively. Glacier oscillations following the LGM maximum position are evidenced in both Rhine and Reuss systems but show varying degrees of preservation. Largely contemporaneous, late LGM readvances of Rhine (Stein am Rhein stadial) and Reuss (Bremgarten stadial) glaciers occurred after 20.6 ± 1.7 ka and 20.8 ± 1.3 ka, respectively. Absence of upstream moraines suggests rapid ice decay without marked stabilization, thereafter. Despite clear differences in the size and nature of their foreland lobes, with Rhein glacier as a broad piedmont lobe and narrow valley glacier like lobes characterising the eastern Reuss system, a remarkable similarity in timing is shown between the two.

1. Introduction

Inception of the theory of the ice ages was based primarily on evidence found in the European Alps (Krüger, 2013 and references therein). Already in the first half of the 19th century, moraines on the northern Alpine foreland were mapped in detail and recognized as delineating past ice margins (Venetz, 1830; de Charpentier, 1835, 1841; Schimper, 1837; Agassiz, 1838). The Alps have one of the most complete data sets globally on the timing of Last Glacial Maximum (LGM) glacier advances (Ivy-Ochs et al., 2004a, 2018; Monegato et al., 2007, 2017; Preusser et al., 2007, 2011; Akçar et al., 2011; Starnberger et al., 2011; Ravazzi et al., 2012, 2014; Castelletti et al., 2013; Reber et al., 2014; Scapozza et al., 2014; Gianotti et al., 2015; Graf et al., 2015; Wirsig et al., 2016; Federici et al., 2017; Wüthrich et al., 2018; Gaar et al., 2019; Braakhekke et al., 2020; Rey et al., 2020; Kamleitner et al., 2022; Ribolini et al., 2022; Roattino et al., 2022; Serra et al., 2022). Nevertheless, crucial knowledge gaps remain, especially in the central part of the northern Swiss foreland, which is dominated by the Reuss and Rhine LGM glacier systems (Fig. 1).

The Rhine glacier is often referred to as a key site for LGM timing in

* Corresponding author.
E-mail address: kamsarah@phys.ethz.ch (S. Kamleitner).

https://doi.org/10.1016/j.geomorph.2022.108548
Received 4 March 2022; Received in revised form 28 November 2022; Accepted 1 December 2022
Available online 7 December 2022

the Northern Alps. Penck and Brückner (1909) differentiated two main moraine complexes of Würmian age (sensu Chaline and Jerz, 1984; today assigned to the LGM (Ellwanger et al., 2011)). This two-phased LGM end moraine model of the Rhine glacier was gradually expanded and subdivided (Schmidt, 1911; Schmidle, 1914; German and Mader, 1976; de Jong, 1983; Hantke, 1983; Moegle, 1994; de Graaff and de Jong, 1995; Keller and Krayss, 2000), wherein authors referred to an assortment of stadial names and numbers. Keller and Krayss (2005a) constructed a chronological framework based on published radiocarbon dates of bones, tusks, and bulk peat. Despite concerns on the validity of such ^{14}C dates (Hedges and Law, 1989; van Klinken, 1999; Collins et al., 2002; Brock et al., 2007a; Hajdas et al., 2007, 2021), the established chronology has not been reviewed critically. More recent age controls are limited to a single local study on LGM outwash sediments (Preusser et al., 2007). In comparison, the smaller Reuss glacier has received less research attention. Three phases of LGM glacier stabilization (Mellingen, Stetten, and Bremgarten stadials) are traditionally differentiated, which were also linked to other lobes in the Reuss glacier system (Fig. 15; Penck and Brückner, 1909; Hug, 1917; Heim, 1919; Hantke, 1983; Keller and Krayss, 1993). Very few numerical ages (luminescence (Gaar et al., 2019), surface exposure (Reber et al., 2014), and radiocarbon (Zbinden et al., 1989; Beckmann, 2004; Graf, 2009; Rey et al., 2020)) are available for the Reuss glacier system.

The aim of this study is to gain an understanding of the behavior of the Rhine and Reuss glaciers during the LGM by reconstructing their ice margins at various points in time. Such data are required to understand large-scale atmospheric patterns and thus forcing mechanisms in Alps paleoclimate, specifically the impact of the Laurentide ice sheet on paleoprecipitation (Luetscher et al., 2015; Monegato et al., 2017; Višnjević et al., 2020; Gribenski et al., 2021; Del Gobbo et al., 2022; Velasquez et al., 2022). This is an issue of some significance as different approaches have led to markedly divergent interpretations with respect to moisture delivery trajectories. Either a situation similar to today's, dominated by westerlies throughout the LGM (Višnjević et al., 2020) or an early phase of dominant meridional moisture transport (Luetscher et al., 2015; Spötl et al., 2021) are discussed. Finally, chronologically well constrained, mapped LGM ice extents provide critical points of validation and ground truthing for Alpine ice cap modelling results (Becker et al., 2016; Seguinot et al., 2018; Imhof et al., 2019) and the regional climate model input functions (Velasquez et al., 2020, 2021, 2022).

Accordingly, we present a detailed reconstruction of the paleo ice margins of the Rhine piedmont glacier and the eastern part of the Reuss glacier system based on high-resolution digital elevation data. Chronological constraints are provided by our new cosmogenic ^{10}Be and ^{36}Cl exposure ages and new radiocarbon dates; key missing pieces to the scattered LGM timing constraints currently available for the northern Alpine foreland. Previously published temporal data for the two glacier systems are critically assessed given methodological advances and findings of recent years. Our geomorphological analysis provides detailed insights into paleoglacier configurations and the interplay of foreland glacier lobes during the LGM. Specific landform interpretation viewed in light of the new dating results permits a deeper understanding of the similarities and differences of Rhine and Reuss glacier dynamics.

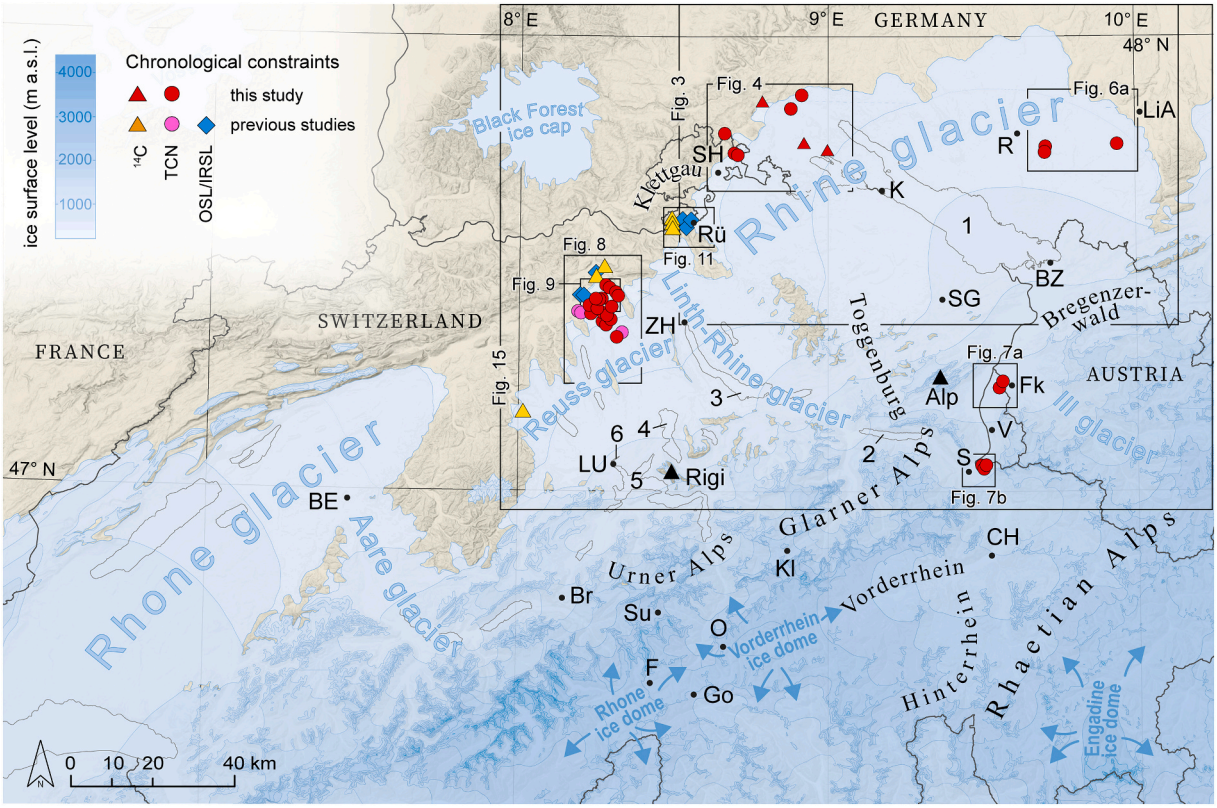

Fig. 1. The northwestern Alpine foreland during the Last Glacial Maximum (modified after Bini et al., 2009; provided by the Federal Office of Topography swisstopo). Published chronological constraints on LGM maximum timing of Reuss and Rhine glacier systems from radiocarbon (^{14}C), surface exposure (TCN), and luminescence (OSL/IRSL) dating are shown. New dates presented in this study are highlighted in red. For specific dates see main text and original publications (Beckmann, 2004; Preusser et al., 2007; Graf, 2009; Gaar et al., 2014, 2019; Reber et al., 2014). Alpine passes: Br: Brünig Pass, Go: Gotthard Pass, F: Furka Pass, Kl: Klausen Pass, O: Oberalp Pass, Su: Susten Pass. Cities: BE: Bern, BZ: Bregenz, CH: Chur, Fk: Feldkirch, K: Konstanz, LiA: Leutkirch im Allgäu, LU: Luzern, R: Ravensburg, S: Sargans, SH: Schaffhausen, V: Vaduz, ZH: Zurich. Peri-alpine lakes: 1: Lake Constance, 2: Lake Walen, 3: Lake Zurich, 4: Lake Zug, 5: Lake Lucerne, 6: Lake Rotsee. Mountain peaks (triangle symbol): Alp: Alpstein massif, Rigi: Rigi mountain. Elevation data provided by European Union, Copernicus Land Monitoring Service 2020, European Environment Agency.

2. Setting

2.1. Rhine glacier system

With a size of ca. 13,500 km^2, Rhine glacier corresponds to one of the largest LGM glacier systems in the Alps. The piedmont lobe itself covered wide areas of northeastern Switzerland and southwestern Germany. The main accumulation areas of the Rhine glacier system encompassed large parts of the Rhaetian Alps, the northeastern section of the Glarner Alps, and the regions of Alpstein and Bregenzerwald (Fig. 1). Highest peaks are located in the southern parts of the catchment and reach up to above 3600 m a.s.l. in the Glarner Alps. At the head of Vorderrhein Valley, the presence of an ice dome reaching ice surface elevations of around 2700 m a.s.l. was reconstructed (Florineth and Schlüchter, 1998). At Sargans, part of Rhine glacier ice branched off towards Lake Walen and formed the Linth-Rhine glacier after confluence with ice masses from the Glarner Alps. At the diffluence, LGM ice surface is estimated to have reached around 1750 m a.s.l. (Hantke, 1968; Jäckli et al., 1970; Bini et al., 2009). The flow of the major Rhine glacier arm continued northwards along the overdeepened Alpenrhein Valley (Jordan, 2010; Schälli, 2012; Pietsch and Jordan, 2014). The term Alpenrhein Valley refers to the Rhine Valley stretch between the confluence of Vorderrhein and Hinterrhein valleys and the upstream end of Lake Constance. The Ill paleoglacier confluenced close to Feldkirch and contributed major ice masses flowing out from the western Austrian Alps. On the foreland, Rhine glacier was joined by ice masses from Toggenburg and the Alpstein massif, as well as from Bregenzerwald (Fig. 1). Rhine glacier advanced into and beyond the basin of Lake Constance and terminated as a wide piedmont glacier (Jäckli, 1962; van Husen, 1987; Ellwanger et al., 2011). Ice flow dynamics and extent of the Rhine glacier were investigated in recent glacier modelling studies (Benz-Meier, 2003; Cohen et al., 2018; Seguinot et al., 2018; Imhof et al., 2019).

2.2. Reuss glacier system

Reuss glacier system (~4000 km^2) is located entirely in central Switzerland (Fig. 1) with ice masses flowing from the Urner and western Glarner Alps (maximum elevations above 3600 m a.s.l.). Major accumulation areas were located in the upper Reuss Valley, encompassed by Susten, Furka, Gotthard, Oberalp, and Klausen passes. Parts of the ice drained towards the basin of Lake Zug with additional input from a right tributary glacier coming from the western Glarner Alps. A second branch of the glacier advanced westwards following present-day Lake Lucerne and merged with left tributary glaciers partly fed by ice from an Aare glacier transfluence over Brünig Pass (1008 m a.s.l.; Bini et al., 2009). North of Rigi mountain, both glacier arms coalesced and advanced onto the northern foreland. Upon reaching the lowlands, Reuss glacier separated into several individual finger-like lobes.

3. Materials and methods

3.1. Field surveys

Fieldwork was carried out in the winter half years from 2018 to 2021. Landform morphology and interrelationships, ideally combined with sedimentological observations, were recorded. Based on published literature and geological maps, the study area was surveyed for large erratic boulders (>1 m in height) in situations suitable for surface exposure dating (Ivy-Ochs and Kober, 2008). Prospection focused primarily on beforehand identified moraine ridges in forested areas. Agricultural land was avoided due to the common destruction and/or displacement of erratics.

3.2. Geodata and GIS landform analysis

Field observations were combined with geomorphological analysis based on remotely sensed data. Elevation data with resolutions up to 0.5 m are freely available for parts of the study area located in Switzerland and Liechtenstein (Federal Office of Topography swisstopo, 2018b). The high-resolution (1 m) relief model of Baden-Württemberg was accessed via a fee-based Web Map Service (WMS) of the Landesamt für Geoinformation und Landentwicklung Baden-Württemberg. The elevation model of Bavaria was purchased from the Bavarian surveying and mapping authority. LiDAR data for Austrian parts of the study area were provided by the Landesamt für Vermessung und Geoinformation of Vorarlberg. High-resolution elevation models and their derivates (e.g. hillshade, slope, aspect models) were used to visualize spatial relations of landforms and to assess the nature and timeline of landscape formation. Geological maps provided additional information for landform analysis. Swiss and Bavarian geological data (1:25,000) are open to the public and made available online by the Federal Office of Topography swisstopo and the Bavarian Environment Agency. The State Office for Geology, Natural Resources and Mining granted access to geological data of Baden-Württemberg (1:50,000; Regierungspräsidium Freiburg Landesamt für Geologie, Rohstoffe und Bergbau, 2013). Geological maps of Austria (1:50,000) are provided by the Austrian Geological Survey via free WMS services.

Esri ArcMap 10.6 software including ArcGIS Spatial Analyst extension was used for all Geographic Information System (GIS) tasks. Post-processing of maps and figures was done in Adobe Illustrator software.

3.3. Surface exposure dating

Sampling of erratic boulders for surface exposure dating was undertaken using angle grinder, hammer, and chisel (Fig. 2). Topographic shielding was recorded using a clinometer and noted down together with sample thickness and boulder location (Tables 1-4). Sample preparation was undertaken at the Laboratory of Ion Beam Physics, ETH Zurich and the Institute of Geological Sciences, University of Bern. Quartz bearing lithologies, permitting ^{10}Be sample preparation, were crushed and sieved to grain sizes <800 μm. For whole rock ^{36}Cl analysis, a grain size range of 250–400 μm was used.

3.3.1. ^{10}Be exposure dating

In order to separate quartz, crushed whole rock samples underwent selective chemical dissolution (Kohl and Nishiizumi, 1992). ^{10}Be was extracted from 23 clean quartz separates following the procedures described in Kronig et al. (2018 and references therein). ^{10}Be/^{9}Be ratios were determined using Accelerator Mass Spectrometry (AMS). AMS measurements were performed on the 0.5 MV Tandy and 0.3 MV Milea machines at the Laboratory of Ion Beam Physics, ETH Zurich. Ratios were normalized relative to the ETH Zurich in-house ^{10}Be standard S2007 N (^{10}Be/^{9}Be ratio of 28.1 × 10^{-12}), which was calibrated relative to the 07KNSTD standard (Christl et al., 2013) and corrected for full process and running mean blank values of 2.74–3.73 × 10^{-15} (Table 3). ^{10}Be exposure ages were determined with the CRONUS Earth online calculator (Balco et al., 2008). The northeastern North American calibration data set (NENA, version 2.2; Balco et al., 2009) and the scaling scheme of Lal (1991) and Stone (2000) were used. Feasibility of the NENA calibration set has recently been demonstrated in Alpine settings (Claude et al., 2014). Internal and external uncertainties are reported as 1σ errors, with the former accounting for AMS errors only. The latter additionally include uncertainties related to ^{10}Be nuclide production rates (Balco et al., 2008). Exposure ages were corrected for an erosion rate of 1 mm ka^{-1} as inferred from postglacial weathering rates based on height differences between glacially polished quartz veins and surrounding rock (André, 2002). Applied erosion correction raises calculated ages by 1.1–4.3 % (median value of 1.5 %) compared to a non-erosion scenario. Erosion corrected ^{10}Be exposure ages range from

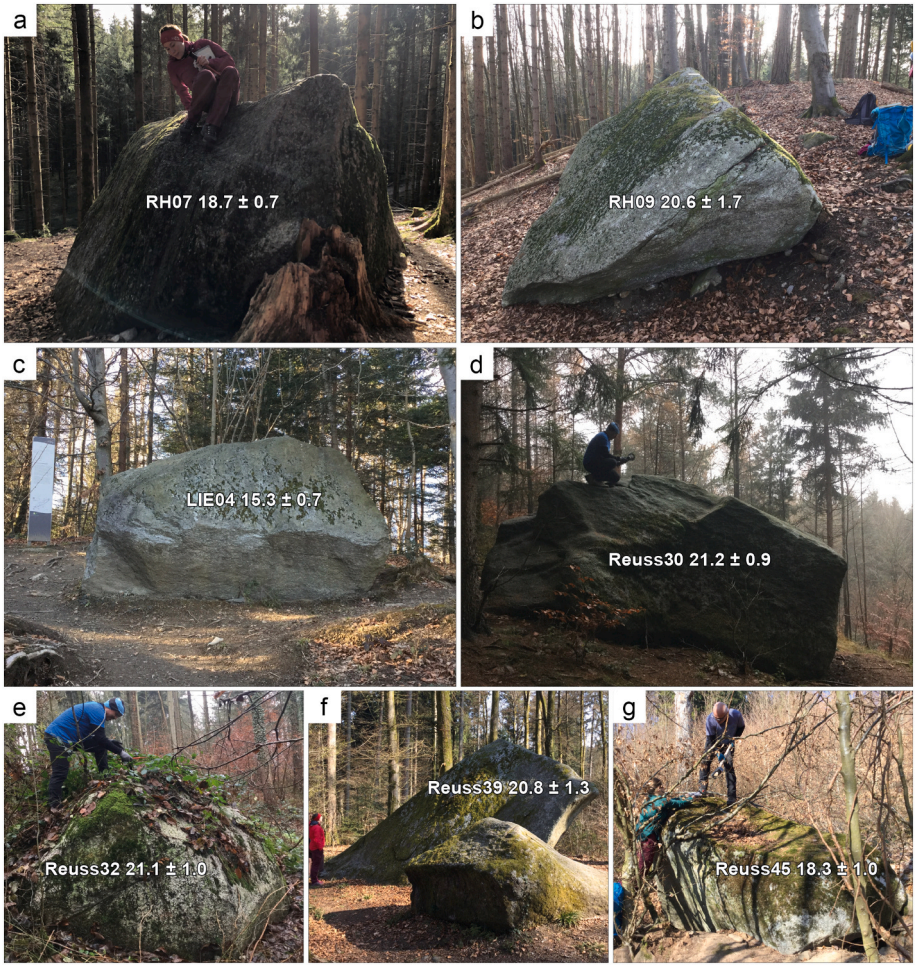

Fig. 2. Erratic boulders from the Rhine (a-c) and Reuss (d-g) glacier systems and their determined surface exposure ages (ka), see also Table 1 and Table 3.

14.1 ± 0.8 ka to 53.6 ± 2.0 ka (Table 3). Due to their low elevation position on the foreland or near the valley bottoms, exposure ages were not corrected for snow cover. Instrumental records insufficiently reflect snow height and duration of snow cover over the past millennia. When projecting the 62 year long record from Chur (556 m a.s.l.; Fig. 1) with an average of 6 cm of snow over 4 months per year (Federal Office of Meteorology and Climatology MeteoSwiss, 2016) into the past, ^{10}Be exposure ages would increase by 0.5 %. Even if significantly larger amounts of snow are assumed, e.g. 50 cm of snow over three months per year, calculated ages would increase by ~3 %, the corrections would remain largely within internal errors. Previously published ^{10}Be exposure dates were recalculated according to the procedure and corrections described above.

3.3.2. *^{36}Cl exposure dating*

Rock samples of non-quartz bearing lithologies or samples with insufficient quartz yield were prepared for whole rock ^{36}Cl dating. Sample preparation closely followed the procedures described in Stone et al. (1996), Ivy-Ochs (1996), Ivy-Ochs et al. (2004b), and summarized in Groos et al. (2021). AMS measurements were conducted using the 6 MV Tandem system at the Laboratory of Ion Beam Physics, ETH Zurich. ^{36}Cl/Cl ratios were measured against the K382/4 N standard with a nominal ratio of 17.36 × 10^{-12} and normalized against KNSTD 5000 (Synal et al., 1997; Christl et al., 2013; Vockenhuber et al., 2019). Measured ratios were corrected for full process blanks of 1.0 × 10^{-15}, 1.9 × 10^{-15}, and 3.3 × 10^{-15} (Table 4). ICP-MS on leached aliquot samples was run by Actlabs (Ontario, Canada). Results from the elemental analysis are given in Table 5. An in-house MATLAB code was used to calculate ^{36}Cl exposure ages. The code implements constants and equations specified in Alfimov and Ivy-Ochs (2009) and uses spallation production rates of 48.8 ± 3.4 at g_{Ca}^{-1} a^{-1} (Stone et al., 1996), 162 ± 24 at g_{K}^{-1} a^{-1} (Evans et al., 1997), 13 ± 3 at g_{Ti}^{-1} a^{-1} (Fink et al., 2000), and 1.9 ± 0.2 at g_{Fe}^{-1} a^{-1} (Stone et al., 2005) and the scaling scheme of Stone (2000). A neutron flux value of 760 n g_{air}^{-1} a^{-1} is used to account for (*epi*) thermal neutron capture on ^{35}Cl (Alfimov and Ivy-Ochs, 2009 and references therein). Production of ^{36}Cl through muon induced reactions in Ca and K amounts to 9 % and 6 %, respectively (Stone et al., 1996, 1998; Evans et al., 1997). The applied parameters are in good agreement with those recently published in geologic calibration studies (Borchers et al., 2016; Marrero et al., 2016). Natural chlorine contents of analysed rock samples range from 175 to 1433 ppm (Table 5). As for ^{10}Be exposure ages, an erosion correction of 1 mm ka^{-1} was applied, lowering calculated ^{36}Cl exposure ages by 0–14 % (Table 4). Due to various production pathways of ^{36}Cl and depending on the individual elemental composition of each sample, erosion correction may differ between samples. As such, the exposure ages of sample RH05 and RH06 were not affected by the specified erosion rates, while for sample RH02 the same correction lowered the exposure age by nearly 11 ka (14 %). Erosion corrected ^{36}Cl exposure ages range from 14.4 ± 1.0 ka to 68.7 ± 2.2 ka (Table 4). No corrections for past snow cover were applied.

3.3.3. *Handling of surface exposure ages*

As a result of moraine degradation, incompletely exposed rock surfaces commonly cause scatter in cosmogenic nuclide datasets (Putkonen and Swanson, 2003; Briner et al., 2005; Ivy-Ochs and Kober, 2008; Heyman et al., 2011). Human impact (e.g. quarrying) may similarly

Table 1
Site information and boulder details of ^{10}Be dated erratics.

Sample ID	Location	Boulder lithology	Boulder size L x W x H	Latitude	Longitude	Elevation
			m	°*N*	°*E*	*m a.s.l.*
RH07[z]	Schaffhausen stadial	Gneiss	4.0 × 3.0 × 2.0	47.7625	9.9390	707
RH08[z]	Schaffhausen stadial	Gneiss	3.0 × 3.0 × 2.2	47.7574	9.7057	743
RH09[z]	Schaffhausen stadial	Gneiss	3.5 × 2.5 × 2.0	47.7572	9.7056	743
LIE02[y]	Alpenrhein Valley	Punteglias granite	4.0 × 2.0 × 2.0	47.0566	9.4951	602
LIE03[y]	Alpenrhein Valley	Punteglias granite	3.3 × 2.5 × 3.0	47.0563	9.4946	611
LIE04[y]	Alpenrhein Valley	Gneiss	3.0 × 2.0 × 3.0	47.2382	9.5629	694
LIE05[y]	Alpenrhein Valley	Gneiss	1.7 × 1.5 × 0.8	47.2395	9.5651	690
Reuss-20[+,v]	Stetten stadial	Granite	2.5 × 1.0 × 1.3	47.3476	8.3144	502
Reuss-21[+,v]	Untertannwald ice margin	Granite	12.0 × 6.0 × 4.5	47.3952	8.1947	446
Reuss-22[+,v]	Untertannwald ice margin	Granite	8.0 × 6.0 × 3.5	47.3955	8.1883	475
Reuss30[w]	Untertannwald ice margin	Granite	5.0 × 3.0 × 3.0	47.4493	8.2785	435
Reuss31[w]	Untertannwald ice margin	Granodiorite	3.5 × 1.5 × 1.8	47.4478	8.2790	424
Reuss32[w]	Mellingen stadial	Granodiorite	3.0 × 1.5 × 2.0	47.4289	8.2654	406
Reuss33[w]	Mellingen stadial	Granite	1.5 × 2.0 × 1.5	47.4278	8.2554	394
Reuss34[w]	Mellingen stadial	Granodiorite	3.0 × 2.0 × 1.0	47.4279	8.2525	393
Reuss35[w]	Mellingen stadial	Granite	1.5 × 1.0 × 1.5	47.3738	8.2713	548
Reuss36[w]	Mellingen stadial	Gneiss	2.0 × 1.5 × 1.5	47.3740	8.2703	545
Reuss37[w]	Mellingen stadial	Gneiss	2.0 × 1.0 × 1.0	47.3876	8.2808	483
Reuss38[w]	Mellingen stadial	Granite	2.0 × 1.3 × 0.5	47.3881	8.2809	480
Reuss39[x]	Stetten stadial	Granite	6.0 × 2.0 × 3.0	47.3449	8.3139	460
Reuss40[x]	Wagenrain	Granite	1.0 × 1.0 × 1.5	47.3959	8.2300	473
Reuss41[x]	Wagenrain	Granodiorite	2.0 × 1.5 × 1.0	47.4023	8.2253	466
Reuss42[x]	Wagenrain	Granodiorite	2.0 × 1.5 × 1.5	47.4077	8.2507	515
Reuss44[x]	Mellingen stadial	Gneiss	2.0 × 2.5 × 1.0	47.4114	8.2973	418
Reuss45[x]	Untertannwald ice margin	Granite	2.5 × 1.0 × 1.5	47.4358	8.3074	531
Reuss46[x]	Untertannwald ice margin	Granite	2.5 × 2.0 × 1.5	47.4406	8.3035	546

[+] Reber et al., 2014.
[v,w,x,y,z] sampled in (v) 2012, (w) 2018, (x) 2019, (y) 2020, (z) 2021.

Table 2
Site information and boulder details of ^{36}Cl dated erratics.

Sample ID	Location	Boulder lithology	Boulder size L x W x H	Latitude	Longitude	Elevation
			m	°*N*	°*E*	*m a.s.l.*
RH02[y]	Schaffhausen stadial	Phonolite	3.0 × 3.0 × 1.2	47.7436	8.6923	433
RH03[y]	Schaffhausen stadial	Phonolite	2.5 × 1.5 × 1.3	47.7397	8.7036	514
RH04[y]	external to LGM	Phonolite	1.5 × 1.5 × 1.6	47.7871	8.6611	572
RH05[y]	Schaffhausen stadial	Permian conglomerate	3.0 × 2.5 × 2.0	47.8416	8.8766	510
RH06[y]	Schaffhausen stadial	Permian conglomerate	5.0 × 3.0 × 1.4	47.8713	8.9115	571
Reuss43[x]	Wagenrain	Amphibolite	8.0 × 6.0 × 4.0	47.3957	8.2698	536

[x,y] Sampled in (x) 2019, (y) 2020.

distort landform stabilization ages towards the younger (Akçar et al., 2011). In contrast, inherited nuclides are encountered much less frequently (Putkonen and Swanson, 2003; Heyman et al., 2011). Apart from the specific cases discussed in Sections 4.1 and 4.2, we generally argue that the oldest exposure age provides the best estimate of the timing of moraine stabilization (Putkonen and Swanson, 2003; Briner et al., 2005). Reduced chi squared statistics and two-tailed generalised extreme Studentized deviate tests, both included in the iceTEA toolkit (Jones et al., 2019), were run to support geologically informed identification of outliers.

3.4. Radiocarbon dating

The present ^{14}C chronology of the LGM Rhine glacier is primarily based on tusk and bone ages (Keller and Krayss, 2005a and references therein). Therefore, locating objects included in the chronology and redating them with modern methods is a key component of this study, especially for the ages constraining the LGM maximum timing on the foreland. Out of these, the Engen mammoth tusk, the Markelfingen mammoth tusk (Fig. 5), and the mammoth skull of Steißlingen were successfully located. The Engen and Markelfingen tusk fragments and the Steißlingen skull are currently stored at the Anne-Frank-Schulverbund in Engen, Germany, the Hegau Museum in Singen, Germany and the Bodensee-Naturmuseum in Konstanz, Germany, respectively and were kindly provided for this study. Using a small drill, two samples (RH-MT-Mkf1; RH-MT-Mkf2) were taken from different points along the untreated Markelfingen tusk fragment (ca. 60 cm long part of the tusk tip, diameter of up to ~10 cm). Two samples (RH-MT-E1; RH-MT-E2) were sampled from the Engen tusk fragment (ca. 30 cm long, diameter of <10 cm). One sample was retrieved from the Steißlingen mammoth skull (RH-MS-St1). An additional sample (RH-MT-StH2) was taken from a mammoth tusk found south of Steißlingen in 2019 (personal communication J. Hald, Kreisarchäologie Konstanz, 2019). This tusk is not part of the Rhine glacier chronology (Keller and Krayss, 2005a).

Radiocarbon dating was performed on the collagen fractions of ivory and bone. Bone sample preparation at the Laboratory of Ion Beam Physics, ETH Zurich was recently summarized in Quarta et al. (2021) and Pawełczyk et al. (2022). The mineral components of bone and ivory were dissolved using 1 M HCl. Base-cleaned gelatine was purified using the ultrafiltration method following Brock et al. (2007b) as described in Hajdas et al. (2009). Freeze dried samples were combusted and

Table 3
Sample details and exposure ages of ^{10}Be dated erratic boulders.

Sample ID	Location	Sample thickness	Topographic shielding factor	^{10}Be concentration	Exposure age* 1 mm ka^{-1} erosion
		cm		*10^5 at g^{-1}*	*ka*
RH07	Schaffhausen stadial	3.0	0.9976	1.347 ± 0.051[e]	18.7 ± 0.7 (1.2)
RH08	Schaffhausen stadial	2.0	0.9997	1.344 ± 0.045[e]	17.9 ± 0.6 (1.1)
RH09	Schaffhausen stadial	2.0	0.9981	1.539 ± 0.124[e]	20.6 ± 1.7 (2.0)
LIE02	Alpenrhein Valley	4.0	0.9865	0.946 ± 0.035[c]	14.7 ± 0.6 (0.9)
LIE03	Alpenrhein Valley	2.0	0.9865	0.937 ± 0.040[c]	14.2 ± 0.6 (0.9)
LIE04	Alpenrhein Valley	2.5	0.9979	1.089 ± 0.046[c]	15.3 ± 0.7 (1.0)
LIE05	Alpenrhein Valley	1.0	0.9969	1.212 ± 0.035[d]	16.9 ± 0.5 (1.0)
Reuss-20[+]	Stetten stadial	4.0	1.0000	1.116 ± 0.54[f]	18.6 ± 0.9 (1.3)
Reuss-21[+]	Untertannwald ice margin	5.0	1.0000	1.244 ± 0.49[f]	22.0 ± 0.9 (1.4)
Reuss-22[+]	Untertannwald ice margin	3.0	1.0000	1.311 ± 0.58[f]	22.2 ± 1.0 (1.5)
Reuss30	Untertannwald ice margin	3.0	0.9987	1.200 ± 0.050[a]	21.2 ± 0.9 (1.4)
Reuss31	Untertannwald ice margin	5.0	0.9985	0.842 ± 0.041[a]	15.2 ± 0.7 (1.0)
Reuss32	Mellingen stadial	5.5	1.0000	1.144 ± 0.052[a]	21.1 ± 1.0 (1.4)
Reuss33	Mellingen stadial	4.0	1.0000	2.810 ± 0.099[a]	53.6 ± 2.0 (3.4)
Reuss34	Mellingen stadial	3.0	1.0000	1.018 ± 0.046[a]	18.6 ± 0.8 (1.2)
Reuss35	Mellingen stadial	5.0	1.0000	1.182 ± 0.047[a]	19.1 ± 0.8 (1.2)
Reuss36	Mellingen stadial	3.0	1.0000	1.281 ± 0.050[a]	20.5 ± 0.8 (1.3)
Reuss37	Mellingen stadial	4.0	1.0000	0.836 ± 0.045[a]	14.1 ± 0.8 (1.0)
Reuss38	Mellingen stadial	2.5	1.0000	1.052 ± 0.055[b]	17.7 ± 1.0 (1.3)
Reuss39	Stetten stadial	3.0	1.0000	1.206 ± 0.074[b]	20.8 ± 1.3 (1.7)
Reuss40	Wagenrain	2.0	1.0000	1.201 ± 0.074[b]	20.3 ± 1.3 (1.6)
Reuss41	Wagenrain	4.0	1.0000	1.012 ± 0.055[b]	17.4 ± 1.0 (1.3)
Reuss42	Wagenrain	4.0	0.9990	1.044 ± 0.059[b]	17.2 ± 1.0 (1.3)
Reuss44	Mellingen stadial	5.0	1.0000	1.103 ± 0.084[b]	20.0 ± 1.6 (1.8)
Reuss45	Untertannwald ice margin	5.0	1.0000	1.112 ± 0.061[b]	18.3 ± 1.0 (1.4)
Reuss46	Untertannwald ice margin	4.0	0.9992	1.346 ± 0.071[b]	21.7 ± 1.2 (1.6)

[+] Reber et al., 2014.
[a,b,c,d,e] Applied blank correction ratios of (a) 3.23 × 10^{-15}, (b) 3.29 × 10^{-15}, (c) 3.73 × 10^{-15}, (d) 3.26 × 10^{-15}, (e) 2.74 × 10^{-15}, (f) 2.90 ± 0.33 × 10^{-15}.
* External uncertainties in brackets.

Table 4
Sample details and exposure ages of ^{36}Cl dated erratic boulders.

Sample ID	Location	Sample thickness	Topographic shielding factor	^{36}Cl concentration	Exposure age* no erosion	Exposure age* 1 mm ka^{-1} erosion
		cm		*10^5 at g$_{rock}^{-1}$*	*ka*	*ka*
RH02	Schaffhausen stadial	1.0	0.9772	50.059 ± 1.605[b]	79.7 ± 2.6 (8.2)	68.7 ± 2.2 (7.6)
RH03	Schaffhausen stadial	2.0	1.0000	20.413 ± 0.716[b]	49.1 ± 1.7 (4.3)	45.8 ± 1.6 (4.3)
RH04	external to LGM	2.0	0.9973	33.794 ± 1.656[b]	33.6 ± 1.6 (4.0)	31.1 ± 1.5 (3.8)
RH05	Schaffhausen stadial	2.0	1.0000	2.842 ± 0.190[c]	14.4 ± 1.0 (2.0)	14.4 ± 1.0 (2.0)
RH06	Schaffhausen stadial	1.5	0.9997	3.151 ± 0.264[c]	15.5 ± 1.3 (2.1)	15.5 ± 1.3 (2.1)
Reuss43	Wagenrain	2.0	1.0000	4.935 ± 0.480[a]	19.9 ± 1.9 (2.7)	19.0 ± 1.8 (2.6)

[a,b,c] Applied blank correction ratios of (a) 1.0 × 10^{-15}, (b) 1.9 × 10^{-15}, (c) 3.3 × 10^{-15}.
* External uncertainties in brackets.

Table 5
Elemental data of ^{36}Cl samples.

Sample ID	Al_2O_3	CaO	Fe_2O_3	K_2O	MgO	MnO	Na_2O	P_2O_5	SiO_2	TiO_2	LOI	Gd	Sm	Th	U	Cl
	wt%	*wt%*	*wt%*	*wt%*	*wt%*	*wt%*	*wt%*	*wt%*	*wt%*	*wt%*	*wt%*	*ppm*	*ppm*	*ppm*	*ppm*	*ppm*
RH02	20.34	1.93	2.77	6.87	0.17	0.218	7.19	0.08	54.71	0.299	4.49	3.0	4.7	64.7	24.9	1006 ± 3
RH03	20.73	2.40	2.69	7.04	0.18	0.225	6.27	0.09	55.93	0.294	4.45	3.0	4.3	62.7	30.6	431 ± 2
RH04	20.33	1.33	2.83	6.99	0.17	0.217	7.58	0.10	55.45	0.294	4.21	2.5	3.7	57.7	27.1	1433 ± 12
RH05	5.90	0.02	2.30	2.50	0.33	0.009	0.06	<0.01	87.24	0.128	1.07	1.8	2.0	6.7	2.0	181 ± 4
RH06	6.89	0.03	3.03	3.12	0.41	0.014	0.07	0.03	85.43	0.165	1.20	1.9	2.2	8.0	2.5	175 ± 2
Reuss43	17.20	8.26	12.55	1.93	4.15	0.242	2.49	0.03	51.10	1.066	1.51	0.6	0.5	0.4	1.8	293 ± 9

* Determined with AMS.

graphitized using the AGE system (Wacker et al., 2010). AMS measurements were performed on the 200 kV Micadas system (Synal et al., 2007). With a yield of 5–6 %, collagen within the samples from the Markelfingen tusk (RH-MT-Mkf1, RH-MT-Mkf2) was found sufficiently preserved with good C/N$_a$ ratios of 3.2 (Table 6). Collagen yield of the Steißlingen tusk sample (RH-MT-StH2) with 1 % was low but C/N$_a$ ratios of 3.2 are well acceptable (van Klinken, 1999). Advanced collagen degradation and high C/N$_a$ ratios between 3.6 and 4.1 of the Engen mammoth tusk samples (RH-MT-E1, RH-MT-E2) and the Steißlingen mammoth skull sample (RH-MS-St1) were observed. In case of the latter, no age could be determined. ^{14}C ages of the Engen, Markelfingen, and Steißlingen tusks (Table 6) were calculated according to Stuiver and Polach (1977). Ages were calibrated using OxCal 4.4 online calibration program (Bronk Ramsey, 2009) and the IntCal20 curve (Reimer et al.,

Table 6
Mammoth specimen radiocarbon (re)dated in this study.

Sample ID	Material	Location	Latitude	Longitude	Depth below surface	Year of discovery	Lab no.	Collagen quality indicator[a]		^{14}C Age BP	Age cal BP
								C/N_a	Yield		
			°N	°E	m				%	*a*	*ka*
RH-MS-St1	Mammoth skull[b]	Steißlingen	47.7752	8.9096	6	1979	ETH-110067	4.1	0.04	-[e]	-[e]
RH-MT-StH2	Mammoth tusk	Steißlingen	47.7741	8.9169	0–10	2019	ETH-110064	3.2	0.96	23,249 ± 82	27.7–27.3
RH-MT-Mkf1	Mammoth tusk[c]	Markelfingen	47.7488	8.9914	8	1978	ETH-110065	3.2	5.05	22,125 ± 73	26.8–26.0
RH-MT-Mkf2	Mammoth tusk[c]	Markelfingen	47.7488	8.9914	8	1978	ETH-110066	3.2	6.32	22,002 ± 72	26.4–26.0
RH-MT-E1	Mammoth tusk[d]	Engen	47.8533	8.7912	3	1982	ETH-126731	3.6	0.58	11,352 ± 56	13.3–13.1
RH-MT-E2	Mammoth tusk[d]	Engen	47.8533	8.7912	3	1982	ETH-126732	3.7	0.20	11,628 ± 41	13.6–13.4

[a] Van Klinken (1999) recommends collagen atomic carbon to nitrogen ratios (C/N_a) ratios from 3.1 to 3.5 and collagen yields of 1 % or greater for quality assessment of bone samples.
[b] The Steißlingen skull was previously dated to 14,800 ± 120 ^{14}C a BP (18.6–17.8 ka cal BP) (Geyh and Schreiner, 1984).
[c] The Markelfingen tusk was previously dated to 18,530 + 1045/−925 ^{14}C a BP (25.3–20.1 ka cal BP) (Geyh and Schreiner, 1984).
[d] The Engen tusk was previously dated to 14,610 ± 90 ^{14}C a BP (18.2–17.5 ka cal BP) (Geyh and Schreiner, 1984).
[e] Insufficient preservation of the collagen fraction prohibited the determination of a reliable ^{14}C age in this study.

2020). Ranges of calendar ages are quoted at 95.4 % probability range.

Attempts to reproduce bone radiocarbon ages originally done in the 1970s to early 1990s have been undertaken in other studies, resulting in ages several thousand years older than the original measurements (Hajdas et al., 2009; Spötl et al., 2018). Issues of contamination (exogenous contaminants) and degradation (bone diagenesis) have led to questioning of the validity of bone ages (van Klinken, 1999; Collins et al., 2002; Hajdas et al., 2007), especially in the age range beyond 20 ka (Hedges and Law, 1989) and when found in gravel sites (Brock et al., 2007a). Observed chronological mismatches imply that young carbon contaminants may have been insufficiently removed from bone samples in earlier studies (Hajdas et al., 2009). Methodological limitations are accompanied by geological queries. Stratigraphic context is oftentimes ambiguous, especially when objects were not discovered in situ but found in the course of gravel exploitation or are rediscovered in museum collections (with scant documentation). The potential of single objects being reworked, especially bone fragments or mammoth teeth, cannot always be excluded. In summary, in order to not pick and choose which bone, tusk, or bulk peat dates fit a certain temporal paradigm, we include in our reconstruction only the radiocarbon dates determined recently and having comprehensive documentation (this study; Preusser et al., 2007; Graf, 2009).

4. Results

4.1. Rhine glacier

Ice marginal landforms of the LGM Rhine glacier are subdivided into two main complexes, an outer moraine set that corresponds to the LGM maximum extent of the glacier and an inner moraine set (Fig. 3). We thereby maintain the two-fold structure proposed by Penck and Brückner (1909) (cf. Ellwanger et al., 2011) and refer to the Schaffhausen and Stein am Rhein stadials, ice margins, or complexes, respectively (cf. Schmidle, 1914). Nevertheless, mapped ice marginal deposits and stadial configurations can slightly vary from previous versions (e.g. Penck and Brückner, 1909; Schmidle, 1914; Hantke, 1983; Keller and Krayss, 2000; Regierungspräsidium Freiburg Landesamt für Geologie, Rohstoffe und Bergbau, 2013).

The fresh frontal moraines of the Schaffhausen stadial stand out distinctly from the smooth landforms of the distal unglaciated (during LGM) surrounding terrain. On this basis, delineation of the piedmont lobe's furthest LGM extent is, especially in the central and eastern sectors, geomorphologically straightforward. Four main glacier lobes are distinguished based upon the position of the sinuous Schaffhausen ice margin: Thur, Untersee, Schussen, and Argen lobes (Fig. 3). Moraines of the upstream Stein am Rhein ice marginal complex are located five to thirteen kilometres internal to the outer Schaffhausen frontal moraines and likewise show a partition in the aforementioned lobes.

Despite the huge (nearly 6000 km^2) area covered by the Rhine piedmont glacier, very few large erratic boulders suitable for exposure dating were identified in this study. Erratic boulders are at best today largely limited to forested areas and frequently show marks of exploitation (cuts, drill holes). This likely reflects the thousands of years of human impact in the area (Keller, 1846a, 1846b; Mühlberg, 1905; de Quervain, 1962; Akçar et al., 2011; Labhart, 2013; Gubler, 2020a). We gathered information on >300 erratics for the Rhine LGM glacier. About one hundred large erratics (length >1.5 m) were found. Of these, twelve boulders qualified for surface exposure dating (Table 1, Table 2).

4.1.1. Thur and Untersee lobes

Wide and hummocky ice margins characterize the largely continuous outer Schaffhausen stadial moraines in the eastern sections of the Untersee lobe (Fig. 3). Towards the west, terminal moraines tend to have more pronounced ridgelines but kettle holes remain a common feature. Westwards of Engen, the outer Schaffhausen stadial ice margin over the course of ca. 50 km comprises mainly moraine fragments. A notable,

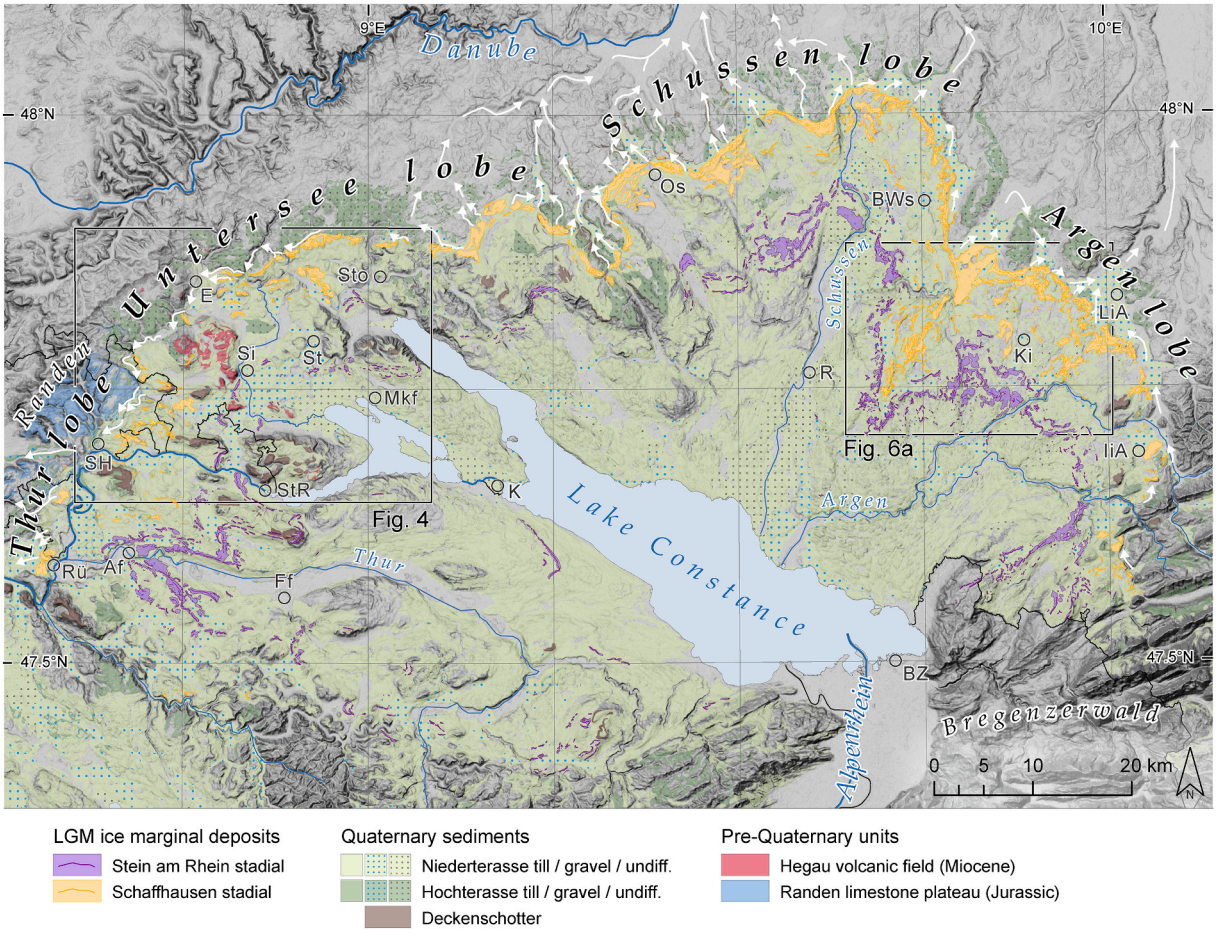

Fig. 3. Ice marginal deposits (Schaffhausen and Stein am Rhein stadials) of the former LGM Rhine glacier on the Swiss-German Alpine foreland (Fig. 1). Main glacier lobes are indicated. White arrows show drainage direction of meltwaters during the LGM maximum position (Schaffhausen stadial) towards Rhine River (Thur and western Untersee lobes) and Danube River (eastern Untersee, Schussen, and Argen lobes), respectively. Geological units modified from the Geological Atlas of Switzerland (Ludwig, 1930; Geiger, 1943, 1968; Eugster et al., 1960; Hübscher, 1961; Saxer, 1965; Hofmann, 1967, 1973, 1981, 1993, 1997; Hottinger et al., 1970; Pavoni et al., 1992; Hantke, 2003; Wyssling, 2007; Zaugg, 2007; Zaugg and Geyer, 2008; Rey et al., 2011; Haldimann et al., 2017) and the Geological Map of Baden-Württemberg (Regierungspräsidium Freiburg Landesamt für Geologie, Rohstoffe und Bergbau, 2013). Niederterrasse refers to Late Pleistocene sediments, Hochterrasse and Deckenschotter to Middle Pleistocene and Early Pleistocene, respectively (Graf and Burkhalter, 2016). Cities: Af: Andelfingen, BWs: Bad Waldsee, BZ: Bregenz, E: Engen, Ff: Frauenfeld, IiA: Isny im Allgäu, K: Konstanz, Ki: Kißlegg, LiA: Leutkirch im Allgäu, Mkf: Markelfingen, Os: Ostrach, R: Ravensburg, Rü: Rüdlingen, SH: Schaffhausen, Si: Singen, St: Steißlingen, Sto: Stockach, StR: Stein am Rhein. Elevation data provided by European Union, Copernicus Land Monitoring Service 2020, European Environment Agency.

several kilometre wide embayment along the frontal moraines is visible in the western section of the Untersee lobe where the ice marginal landforms follow a trace along the upstream side of Hohenstoffeln (~840 m a.s.l.), an eroded volcanic neck of the Hegau volcanic field (Fig. 4). On the steep S-SE facing slopes of the Randen plateau (made up of Jurassic limestones) moraine ridges are missing completely (Fig. 3). Only at two sites south of the city of Schaffhausen are outermost moraines (Schaffhausen stadial) of the Thur lobe morphologically well identifiable. Among them is the terminal moraine set north of Rüdlingen that is characterized by indistinct ridges, hummocky and kettled terrain. Extensive outwash deposits are located at Rafzerfeld plain just to the west. Prominent paleochannels run parallel to the outermost Schaffhausen ice margin. The channel courses can be followed from Engen to south of Altdorf, and via Thayngen to south of Schaffhausen (Fig. 3, Fig. 4), from where waters drained into Klettgau (Fig. 1).

At the city of Engen, pronounced terminal moraines ridges are lacking but the maximum position of the Rhine glacier is determined on sedimentological basis. On site a diamicton with striated clasts and overlain by a 50 cm thick weathering horizon is present and interpreted as till (Geyh and Schreiner, 1984). Within the till layer, a mammoth tusk fragment was found in 1982 during construction works in about 3 m depth (Geyh and Schreiner, 1984). Two samples of the tusk fragment (RH-MT-E1, RH-MT-E2) were newly radiocarbon dated to 11,352 ± 56 ^{14}C a BP (13.3–13.1 ka cal BP) and 11,628 ± 41 ^{14}C a BP (13.6–13.4 ka cal BP). Dating applied after the excavation of the tusk yielded a distinctly older age of 14,610 ± 90 ^{14}C a BP (18.2–17.5 ka cal BP; Hv-11,569; Geyh and Schreiner, 1984). Colluvial origin of the surrounding till was excluded and no signs of artificial burial were detected at the site (Geyh and Schreiner, 1984). Given the young ages, neither of the aforementioned radiocarbon datings can be reconciled with the depositional context of the tusk, which was located right at the outermost LGM ice margin. In fact, bone collagen quality indicators tested in this study clearly point to poor preservation of the Engen tusk (Section 3.4; Table 6) and challenge the reliability of the datings. Accordingly, we do not consider the ^{14}C date of the Engen tusk any further in this text.

Several hundred metres upstream of the outermost ice marginal deposits, a 530 m a.s.l. high hill rises southwest of Thayngen (Fig. 4). Mesozoic limestones and older gravel deposits are seen to underlie a thin, patchy cover of glacial sediments (Hübscher, 1961). Two phonolite erratic boulders (RH02, RH03) located on this bedrock high were dated with ^{36}Cl. Boulder RH02 (68.7 ± 2.2 ka) is located on top of a limestone spur protruding from the western slope of the hill. Sample RH03 (45.8

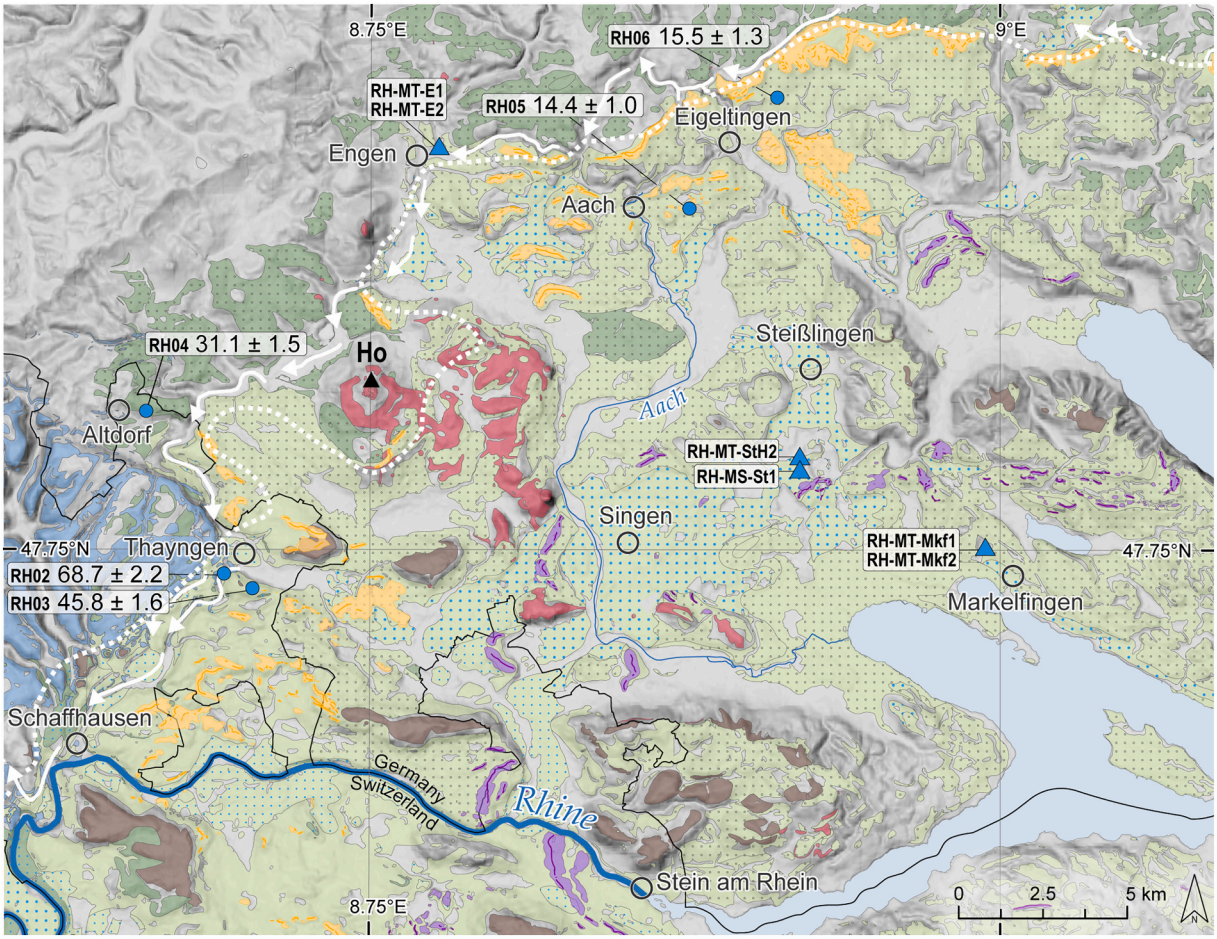

Fig. 4. Close up of the eastern Thur lobe and the western Untersee lobe in the western section of the Rhine glacier piedmont lobe (Fig. 1, Fig. 3). Blue circles indicate locations of sampled erratic boulders (ages given in ka; Table 4). Blue triangles show where the dated Engen mammoth tusk (RH-MT-E1: 13.3–13.1 ka cal BP, RH-MT-E2: 13.6–13.4 ka cal BP), the Markelfingen mammoth tusk (RH-MT-Mkf1: 26.8–26.0 ka cal BP, RH-MT-Mkf2: 26.4–26.0 ka cal BP), and the Steißlingen mammoth tusk (RH-MT-StH2: 27.7–27.3 ka cal BP) and skull (RH-MS-St1: collagen preservation not sufficient for age determination) were found (Table 6). White arrows indicate meltwater drainage towards Rhine River during LGM maximum (Schaffhausen stadial). White dashed line shows the extent of the LGM maximum glaciation after Bini et al. (2009). Geological units modified from the Geological Atlas of Switzerland (Hübscher, 1961; Hofmann, 1981, 1997; Zaugg and Geyer, 2008) and the Geological Map of Baden-Württemberg (Regierungspräsidium Freiburg Landesamt für Geologie, Rohstoffe und Bergbau, 2013). For colour codes please consult Fig. 3. Mountain peak (black triangle symbol): Ho: Hohenstoffeln. Elevation data provided by European Union, Copernicus Land Monitoring Service 2020, European Environment Agency.

± 1.6 ka) lies on the hill's flat top. In contrast to RH02 and RH03, boulder RH04 (31.1 ± 1.5 ka) is located two kilometres external to the mapped LGM outer moraines. The three dated phonolite boulders originate from the nearby Hegau volcanic field (Fig. 4; Schreiner, 1992b) and were glacially scoured and transported a few kilometres northwestwards. Determined exposure ages are older than the timing of the LGM in the Alps and inconsistent from the dates of this and other northern Alpine foreland sites (e.g. Wirsig et al., 2016; Ivy-Ochs et al., 2022). We therefore interpret the boulders to contain high amounts of inherited ^{36}Cl, especially given the deep production mechanisms of ^{36}Cl from muon and neutron capture events (Stone et al., 1996; Gosse and Phillips, 2001; Dunai, 2010). The boulders may have been sourced from shallow spots within the bedrock (less than a few metres), and the outer parts of the boulder may have been insufficiently removed because of limited abrasion over the short transport distance. Alternatively, the high ^{36}Cl concentrations in the phonolite boulders could have built up after deposition in an earlier (pre-LGM) glaciation. Boulders RH02 and RH03 were further identified as outliers within the cosmogenic data set of the Schaffhausen stadial ice marginal complex (Table 1-4) using iceTEA (Jones et al., 2019). Boulder RH04 is located external to the LGM ice margin. The ages for the three boulders are not discussed further.

Numerous moraine fragments are found upstream from the outer Schaffhausen stadial moraines (e.g. between Schaffhausen and Thayngen; between Engen and Eigeltingen). Two samples were collected from such ridges east of the city of Aach (RH05) and northeast of the town of Eigeltingen (RH06) (Fig. 4). RH05 was deposited along an ice margin roughly 2.5 km internal to the outer Schaffhausen moraines. The erratic, locally known as 'Grauer Stein', was dated to 14.4 ± 1.0 ka. Less than one kilometre internal to the LGM maximum margin, RH06 was sampled from an erratic boulder situated on a flat, forested area. With dimensions of ca. 5.0 × 3.0 × 1.4 m, boulder RH06 (15.5 ± 1.3 ka) is the largest erratic sampled on the Rhine foreland. Radiocarbon dates from numerous sites on the northern foreland underline that the Alps were ice free by 19–18 ka (see Section 5.3; Rey et al., 2020). Notably, removing boulder ages RH05 and RH06 from the Schaffhausen ice marginal complex dataset lowers the reduced chi-squared value significantly indicating they belong to a different population (Heyman et al., 2016; Jones et al., 2019). Both of these young exposure ages are likely related to exhumation of the boulders or to human impact and thus are not discussed further in the text.

The Stein am Rhein moraine complex is exceptionally well-developed at the Thur lobe (Fig. 3). It spreads over a longitudinal distance of seven kilometres and can be traced for several tens of kilometres

laterally. In contrast, the Stein am Rhein stadial moraines of the Untersee lobe are less prominent and more strongly fragmented. Except for two several kilometre long ridges west of Lake Constance (Fig. 3), moraines upstream of the Stein am Rhein position, are not observed.

Numerous gravel pits are located south of Steißlingen within the broad band of moraines of the Stein am Rhein ice margin. Mammoth fragments were found within interbedded sands and gravels. A mammoth skull found in 1979 was located approximately six metres below the surface (Geyh and Schreiner, 1984). In 2019, a ca. 40 cm long fragment of a mammoth tusk with a diameter of roughly 15 cm was excavated from a neighbouring pit (0–10 m below the surface; personal communication J. Hald, Kreisarchäologie Konstanz, 2019). Due to insufficient collagen preservation, no age could be determined for the Steißlingen mammoth skull (RH-MS-St1; Table 6). Radiocarbon dating performed on the skull after its discovery in the late 1970s gave an age of 14,800 ± 120 ^{14}C a BP (18.6–17.8 ka cal BP; Hv-10,654; Geyh and Schreiner, 1984). The Steißlingen mammoth tusk (RH-MT-StH2) was radiocarbon dated to 23,249 ± 82 ^{14}C a BP (27.7–27.3 ka cal BP). The possibility that the tusk was reworked cannot be completely excluded, therefore, we do not place it in a central position in our discussion (Section 5.1).

About six kilometres upstream of the Steißlingen pits, a 50 m thick gravel deposit (Schreiner, 1968) is exposed in the Lerchental gravel pit northeast of Markelfingen (Fig. 4). The Markelfingen gravels are drumlinized and overlain by several metres of glacial till (Schreiner, 1968, 1973; Ellwanger, 1990, 1992). In November 1978, a mammoth tusk was found eight metres below the surface, embedded in the gravels (Fig. 5). Large parts of the reportedly complete tusk were destroyed during excavation (personal communication J. Hald, Kreisarchäologie Konstanz, 2019) and suggests little to no reworking. Our new radiocarbon datings (Table 6) yield ^{14}C ages of 22,125 ± 73 ^{14}C a BP (RH-MT-Mkf1: 26.8–26.0 ka cal BP) and 22,002 ± 72 ^{14}C a BP (RH-MT-Mkf2: 26.4–26.0 ka cal BP). The previously determined date for a fragment of the same tusk is 18,530 + 1045/−925 ^{14}C a BP (25.3–20.1 ka cal BP; Hv-10,655; Geyh and Schreiner, 1984).

4.1.2. Schussen and Argen lobes

Eastwards of Engen, the LGM maximum frontal moraines (Schaffhausen stadial) undulate over 150 km and run almost continuously to Isny im Allgäu (Fig. 3). A distinct five kilometre wide and seven kilometre deep embayment in the trend of the ice margin is evident between Untersee and Schussen lobes, separating western and eastern sections of the Rhine glacier. As along Untersee lobe, the morphological character of the frontal moraines of Schussen and Argen lobes changes frequently over short distances. Narrow (ca. 70–200 m wide) and prominent single or double crested moraines that typically reach 10–20 m, rarely even up to 30 m in height, alternate with several hundred metre wide successions of numerous closely spaced short ridges, or chaotic terrain with kettle holes. Wide outwash plains connect downstream of the LGM maximum frontal moraines. Numerous moraines are located upstream from the outer Schaffhausen ice margin (Fig. 3). These ridges can frequently be followed for hundreds of metres but do not connect at or beyond the lobe scale.

A particularly striking feature is the former suture zone between the Schussen and Argen lobes (Fig. 3). This is seen as moraine ridges that trend inwards from and perpendicular to, yet roughly contiguous with, the frontal moraines (Fig. 6). The suture zone encompasses a succession of right and left lateral moraines of Schussen and Argen lobes, respectively. Lateral ridges are well-preserved over 13 km and are assigned to the Schaffhausen moraine set. Close to the town of Waldburg, a double crested right lateral moraine of the Schussen lobe bears several gneiss erratics. While other boulders show severe signs of quarrying, two gneiss erratics were found suitable for surface exposure dating. Only thirty metres apart from each other, the boulders are situated at ca. 740 m a.s.l. Erratic RH09 (Fig. 2b; 20.6 ± 1.7 ka) is found on the highest point of the crest. RH08 (17.9 ± 0.6 ka) is located on the same ridge's northern slope (Fig. 6b).

Five to seven kilometres upstream of the Schaffhausen terminal moraines at Leutkirch im Allgäu, a sequence of multiple, shorter ridges is banked up against a topographic high (Fig. 3). Sample RH07 was taken from a prominent gneiss boulder, located on top of a 250 m long and 10 m high moraine, 1.5 km northeast of Waltershofen (Fig. 6a). The erratic (Fig. 2a) is locally known as 'Heiliger Stein' and was dated to 18.7 ± 0.7

Fig. 5. Photographs of the radiocarbon dated Markelfingen mammoth tusk in its in situ position. The mammoth tusk was found in 1978 in a gravel pit near Markelfingen (location Fig. 4). As seen on the photographs (Kreisarchäologie Landratsamt Konstanz, photographs: Jörg Aufdermauer), the tusk was found in a section of interbedded thick to medium bedded gravels and sands that have been interpreted as advance gravels ('Vorstoßschotter'; Geyh and Schreiner, 1984). The tusk was found in the uppermost section of the gravels, which are in turn overlain by 2–6 m of massive subglacial till. The landscape was reshaped into drumlins (Ellwanger, 1990, 1992).

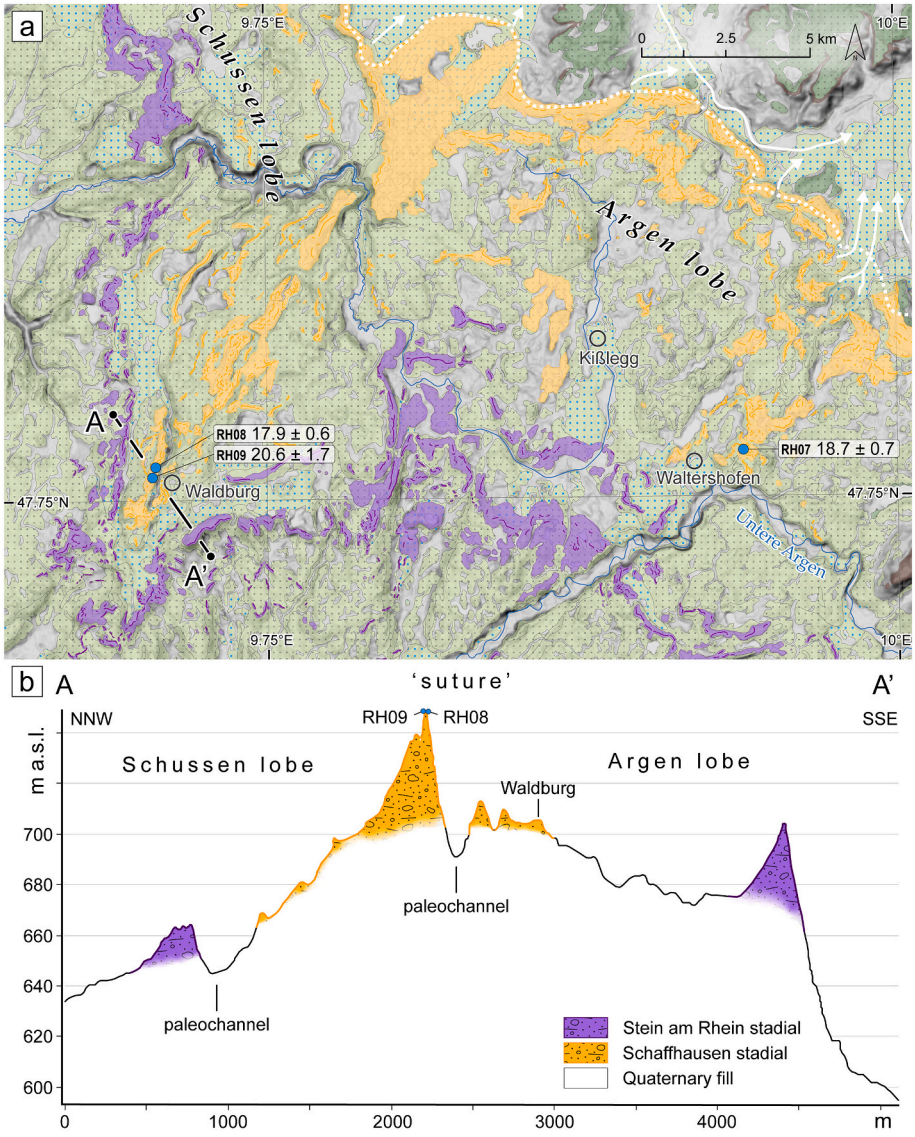

Fig. 6. (a) Close up of the eastern Schussen and western Argen lobes in the eastern section of the Rhine glacier piedmont lobe (Fig. 1, Fig. 3). Topography of the cross-section (A-A') is shown in Fig. 6b. Locations of sampled erratic boulders (blue circles) and their respective ^{10}Be surface exposure ages (ka; Table 3). White arrows indicate meltwater drainage during LGM maximum towards Danube River. White dashed line shows the extent of the LGM maximum glaciation modified after Bini et al. (2009). Quaternary units modified from the Geological Map of Baden-Württemberg (Regierungspräsidium Freiburg Landesamt für Geologie, Rohstoffe und Bergbau, 2013). For colour codes please consult Fig. 3; (b) Cross-section (A-A') of the suture at the lateral contact of Rhine glacier's Schussen and Argen lobes. Location of the cross-section is indicated in Fig. 6a. Locations of dated erratic boulders are indicated by blue circles. Surface of the underlying Molasse bedrock is interpreted to be at elevations between 460 and 560 m a.s.l. (GeoMol Team, 2015). Vertical exaggeration is approximately 15×. Elevation data provided by European Union, Copernicus Land Monitoring Service 2020, European Environment Agency.

ka.

The Stein am Rhein ice margins are preserved quasi continuously along the Schussen and Argen lobes as a several kilometre wide set of multiple moraines. In places, the transition between the Schaffhausen and the Stein am Rhein ice marginal complex can be gradual and morphologically ambiguous. Upstream of the Stein am Rhein position only a few scattered moraine fragments are found (Fig. 3). No boulders suitable for exposure dating were located in this region.

4.1.3. Alpenrhein Valley

Between Sargans and the mouth of Lake Constance (Fig. 1), several bedrock highs protrude from the Alpenrhein valley floor. Among them is Eschnerberg (698 m a.s.l.), which overlooks the present-day valley bottom by up to 260 m (Fig. 7a). A thin cover of glacial sediments overlies the Cretaceous limestone (Eugster et al., 1982), but large erratic boulders are rarely found in situ. On the flat top of Eschnerberg two gneiss boulders were sampled for surface exposure dating, among them is the prominent 'Findling am Gantenstein' (LIE04, Fig. 2c). Exposure ages of LIE04 and LIE05 were determined to 15.3 ± 0.7 ka and 16.9 ± 0.5 ka (Table 3).

Twenty kilometres upstream, close to the city of Sargans and at the former Rhine glacier diffluence (Fig. 7b), Fläscher Berg, another isolated bedrock ridge, overtops Alpenrhein Valley (~490 m a.s.l.) by nearly 650 m. Fläscher Berg is made of Jurassic and Cretaceous limestones (Löpfe et al., 2018) and thinly covered with glacial sediments. Erratic boulders larger than one cubic metre are present sporadically. On site, bedrock is very shallow and no distinct ice margins were recognized. Two of the largest erratic boulders (Punteglias granites) on the northern slopes of Fläscher Berg mountain, were dated (LIE02: 14.7 ± 0.6 ka; LIE03: 14.2 ± 0.6 ka).

4.2. Reuss glacier

The glacial landforms in Bünz Valley and in particular Reuss Valley are well-preserved and rich in morphological detail (Fig. 8). The eastern Reuss glacier lobe comprises three ice marginal complexes; a LGM maximum stadial and two internal stadials. The LGM maximum complex is further subdivided into: (a) an outer LGM maximum position with a low-relief ice margin that is only weakly seen in the landscape (Untertannwald moraines; Fig. 9) and (b) an inner LGM maximum ice margin with a prominent, largely continuous sequence of frontal moraines in a slightly more internal position (Mellingen stadial; Fig. 9). Several kilometres upstream, the Stetten and Bremgarten stadials consist of multiple sub-parallel moraine ridges.

Fig. 7. Eschnerberg (a) and Fläscher Berg (b) bedrock in the Alpenrhein Valley (Fig. 1). Fläscher Berg is located at the former Rhine glacier diffluence. Surface exposure ages from dated erratic boulders (blue circles) are given in ka (Table 3). Quaternary units modified from the Geological Atlas of Switzerland (Eugster et al., 1982; Ibele et al., 2016; Löpfe et al., 2018) and Heissel et al. (1967). For colour codes please consult Fig. 3. Roche moutonnées (red dotted line) on Eschnerberg indicate direction of paleo ice flow. Elevation data provided by the Federal Office of Topography swisstopo and the Landesamt für Vermessung und Geoinformation of Vorarlberg.

4.2.1. LGM maximum: Untertannwald ice margin and Mellingen stadial

Faint ridges and minor hummocky landforms (Fig. 8, Fig. 9) are the geomorphological expression of the LGM maximum lobe extents in Reuss and Bünz valleys. The low-relief moraine deposits group in a several hundred metre wide arcuate band that extends from east of Lenzburg to Othmarsingen in Bünz Valley and from Mägenwil to Untertannwald in Reuss Valley and are hereafter also referred to as Untertannwald ice margin. No moraines are present outboard of this ice margin (Fig. 9). Southwest of Dättwil two large erratic boulders associated with this subtle frontal ice margin (Graf et al., 2007; Bini et al., 2009) were exposure dated to 21.2 ± 0.9 ka (Reuss30; Fig. 2d) and 15.2 ± 0.7 ka (Reuss31). Distinct lateral moraine ridges associated with this position are missing but erratic boulders are found scattered along the west and southwest slopes of Heitersberg (Fig. 8). Out of these, two boulders suitable for surface exposure dating were found at 531 m a.s.l and 546 m a.s.l., and yield ages of 18.3 ± 1.0 ka (Reuss45; Fig. 2g) and 21.7 ± 1.2 ka (Reuss46). We relate them to the low-relief frontal ice margins at Untertannwald, yet cannot rule out completely that the boulders were deposited during a slightly larger ice extent. Reuss31 and Reuss45, based on both statistical treatment (Jones et al., 2019) and geological considerations, are classified as outliers and were likely affected by post-depositional processes.

The northern end of the Wagenrain Molasse ridge that separates Bünz and Reuss valleys, reaches maximum elevations of around 590 m a.s.l. (Fig. 8). Its surface topography is smooth and geomorphological evidence of fresh glacial landforms is lacking. Four erratic boulders at the northern tip of Wagenrain were exposure dated but lack clear association with an ice margin. Out of these, two erratic boulders (Reuss42, Reuss43) stem from a glacial deposit previously assigned to a pre-LGM ('Riß') glaciation (Jäckli, 1966). ^{10}Be ages of 20.3 ± 1.3 ka, 17.4 ± 1.0 ka, 17.2 ± 1.0 ka (Reuss40–42), and one ^{36}Cl age of 19.0 ± 1.8 ka (Reuss43) were obtained.

The Mellingen ice margin in Reuss Valley consists of up to five closely spaced lateral and frontal moraine ridges that enclose the basin of Mellingen (Fig. 8, Fig. 9). The outer deposits of the Mellingen sequence consist of two major frontal moraines and one right lateral moraine, each about 1.3 to 1.6 km long. In comparison to the 1–5 m high ridges of the Untertannwald ice margin, the Mellingen frontal moraines stand out by their large dimensions (Fig. 9). The Mellingen ridges in Reuss Valley are typically 5–35 m in height and have sharp crests. Three erratic boulders were sampled from the prominent inner frontal moraines of Mellingen (Fig. 8). ^{10}Be surface exposure ages are 21.1 ± 1.0 ka (Reuss32), 53.6 ± 2.0 ka (Reuss33), and 18.6 ± 0.8 ka (Reuss34). Boulder Reuss33 is classified as a statistical outlier and likely contains inherited ^{10}Be, perhaps it was remobilized during the LGM. Along the right lateral moraine of the innermost Mellingen complex, a boulder was dated to 20.0 ± 1.6 ka (Reuss44). A series of well-preserved left lateral moraines of the Mellingen stadial can be traced from the frontal moraines in Reuss Valley to the apex of the Wagenrain bedrock ridge (Fig. 8). These are the highest elevation glacial landforms observed on the Wagenrain Molasse hill. Boulders Reuss35 (19.1 ± 0.8 ka) and Reuss36 (20.5 ± 0.8 ka) are located on moraines along the south side of this hill. On the adjacent inner moraine two boulders yielded ages of 14.1 ± 0.8 ka (Reuss37) and 17.7 ± 1.0 ka (Reuss38). Removing Reuss37 from the Mellingen dataset markedly lowers the reduced chi-squared value indicating it does not belong to that population (Heyman et al., 2016; Jones et al., 2019). It was likely exhumed.

In Reuss Valley, the frontal moraines of the Mellingen stadial are accompanied by several meltwater channels (Fig. 9). In the western parts, four generations of paleochannels can be differentiated based on channel elevations, drainage direction, and their positions relative to the former ice margins. West of Birrhard, braided paleochannels of Birrfeld plain cut across the Untertannwald low-relief ridges and the outer Mellingen moraines. A higher and a lower Birrhard paleochannel (Fig. 10a) run internally to the outer Mellingen frontal moraines to the north. Both channels are cut off by the present-day course of Reuss River. The channel elevation offset between the two Birrhard channels is up to ten metres. The 150 to 500 m wide Münzel paleochannel follows internally. The Münzel channel emerges from a breach through the inner left lateral Mellingen moraines, turns to the north and continues parallel to the inner Mellingen frontal moraines. Like the Birrhard paleochannels, the Münzel channel terminates at the present channel of Reuss River. The Mellingen frontal moraines are breached along two narrow (ca. 300 m and 600 m wide) cuts. Present-day Reuss River crosses

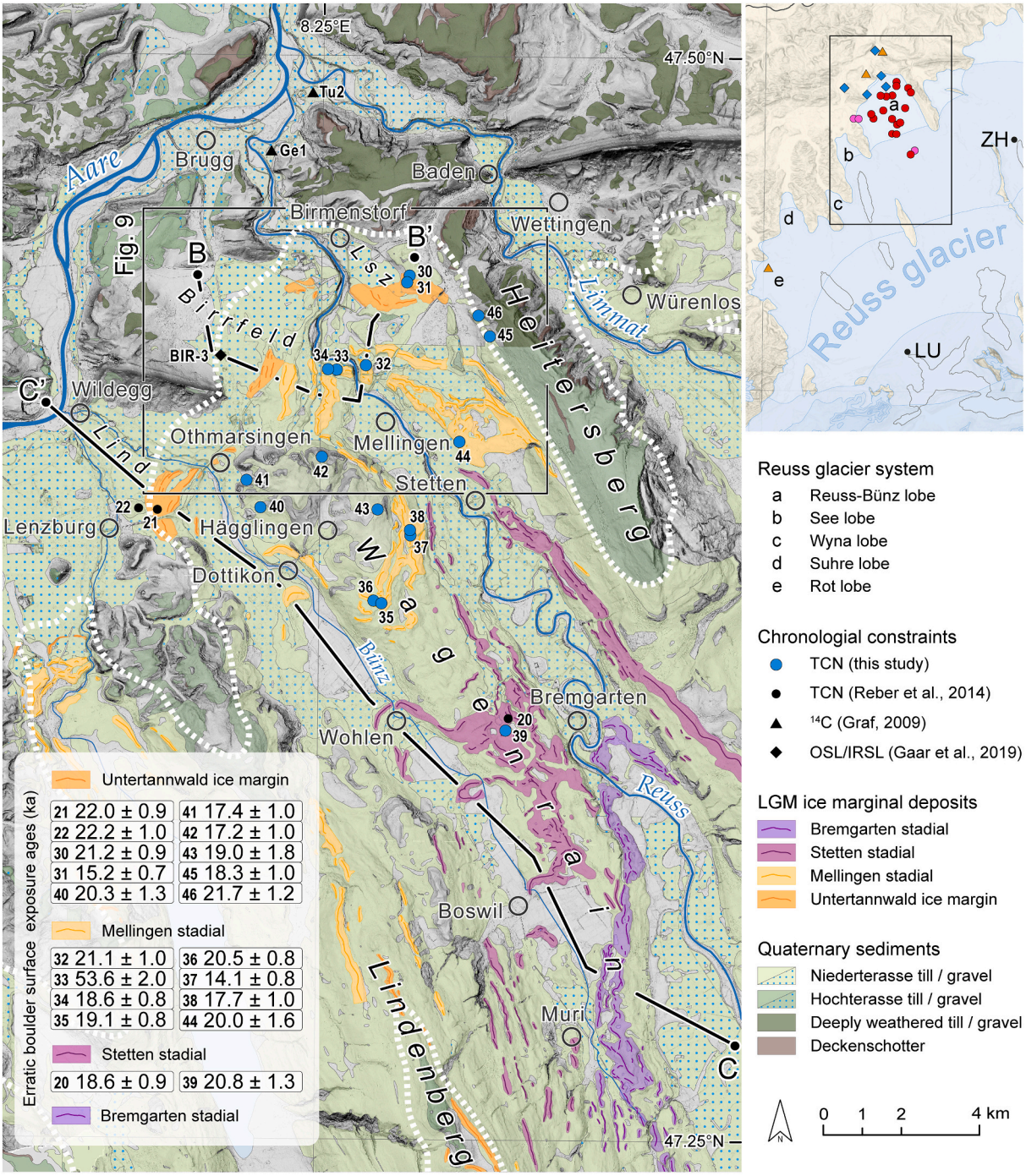

Fig. 8. Ice marginal deposits of the LGM Reuss glacier lobe with downstream outwash plains (Lsz: Lindenstaldenzelg). LGM maximum frontal moraines in Bünz and Reuss valleys correspond to the low-relief Untertannwald ice margin. White dashed line shows the extent of the LGM maximum glaciation (lobes from Reuss and Bünz valleys after Bini et al. (2009)). Highest peaks of the northern end of the Wagenrain bedrock ridge might have protruded from the ice during LGM. Surface exposure ages (TCN) of this study (Table 3, Table 4) and Reber et al. (2014) are shown together with available chronological constraints from radiocarbon (Graf, 2009) and OSL/IRSL datings (Gaar et al., 2019). Geological units modified from the Geological Atlas of Switzerland (Jäckli, 1966; Diebold et al., 2005; Graf et al., 2007, 2012; Jordan et al., 2011; Gubler, 2020b). Niederterrasse refers to Late Pleistocene sediments, Hochterrasse to Middle Pleistocene, respectively (Graf and Burkhalter, 2016). Indicated cross-sections (B-B′, C-C′) are shown in Fig. 10a,b, respectively. The legend to the index map can be found in Fig. 1. Elevation data provided by the Federal Office of Topography swisstopo.

through the western of these two gaps, while the eastern opening connects to the Tanklager paleochannel (Fig. 9, Fig. 10a).

In terms of morphology, size and preservation, the gentle ice margins associated with the Mellingen stadial in Bünz Valley differ strongly from the clear moraine complex in Reuss Valley (Fig. 8, Fig. 10b). Only remnants of a right lateral-frontal moraine ridge can be identified north of the town of Dottikon. About 1.2 km internally, fragments of a frontal and a left lateral moraine follow. A deep onset of a meltwater channel, in which present-day Bünz stream runs, is located between the two moraines at Dottikon (Mellingen stadial; Fig. 8).

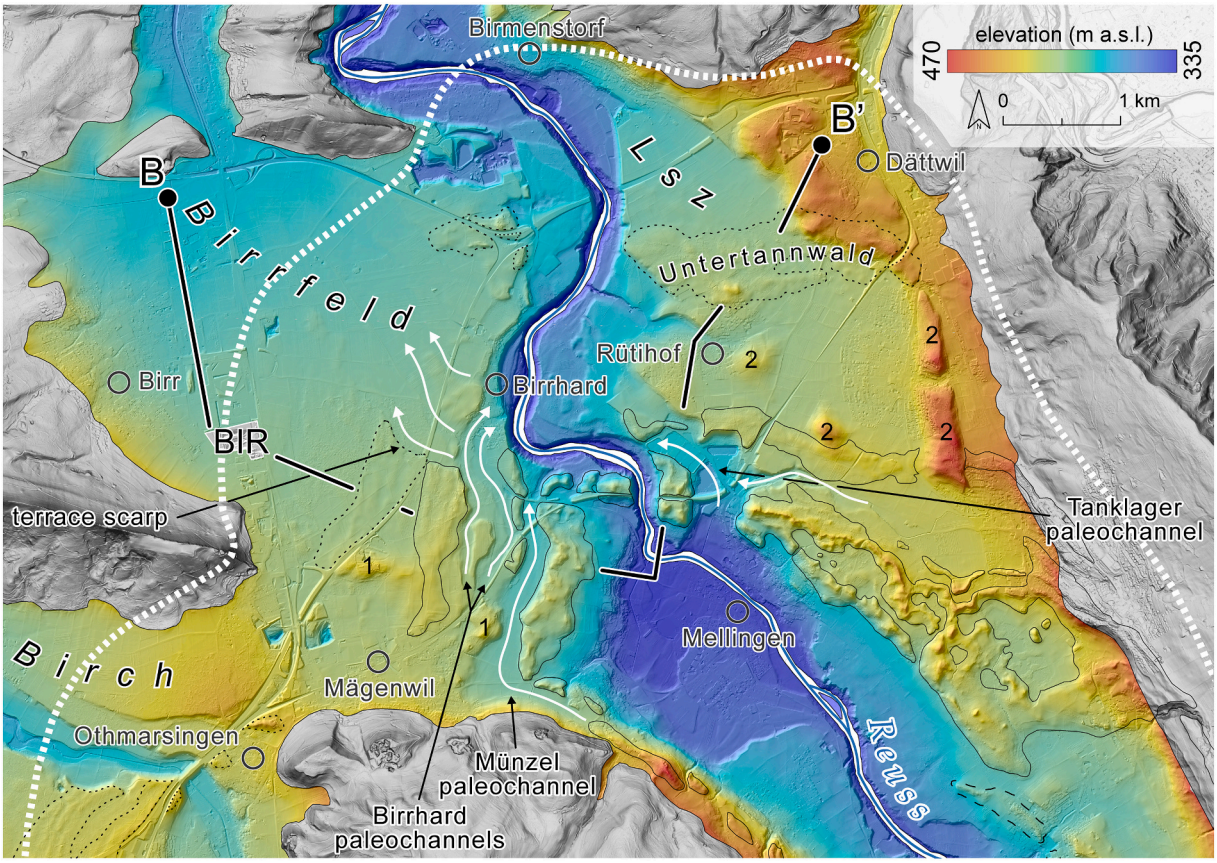

Fig. 9. Ice marginal deposits at the snout of the former LGM Reuss lobe (Fig. 1, Fig. 8). Outwash plains of Birch, Birrfeld, and Lindenstaldenzelg (Lsz) are visible downstream of the low-relief frontal moraines of the LGM maximum position (Untertannwald ice margin; dotted outline). Internally, the prominent end moraines of the Mellingen stadial (solid outline) connect. In the lower right corner of the figure, a frontal moraine ridge of the Stetten stadial is visible (dashed outline). White dashed line shows the extent of the LGM maximum glaciation after Bini et al. (2009). Paleodrainage is indicated by white arrows. A glacial diamicton exposed in Birr 'Joriacher' gravel pit (BIR) was OSL and IRSL dated to LGM (Gaar et al., 2019). For locations of dated erratic boulders refer to Fig. 8. Numbers 1 and 2 highlight Molasse bedrock and old gravel deposits, respectively, thinly draped with LGM till. The black line shows the location of the cross-section (B-B') of Fig. 10a. Elevation data provided by the Federal Office of Topography swisstopo.

4.2.2. *Stetten and Bremgarten stadials*

Four kilometres upstream of the Mellingen stadial moraines at Mellingen (Reuss Valley) and Dottikon (Bünz Valley), up to four distinct moraines of the Stetten stadial can be differentiated in both valleys (cf. Jäckli, 1966). In Reuss Valley, the subparallel right lateral moraine ridges of the Stetten ice margin are particularly prominent. Single lateral moraines reach up to 30 m in height. Frontal moraine ridges are preserved only in the case of the outer Stetten ice margin. Frontal moraines of the inner Stetten positions are missing. Multiple paleochannels run parallel to the left and right Stetten lateral moraines. On top of the Wagenrain saddle (between the towns of Wohlen and Bremgarten, Fig. 8), multiple lateral and frontal moraines spread over a distance of five kilometres (Fig. 8). Organization of moraine ridges is chaotic, the terrain is hummocky with numerous kettle holes and scattered erratic boulders. Reuss39, a large granite boulder (Fig. 2f), yielded a surface exposure age of 20.8 ± 1.3 ka. In the adjacent Bünz Valley, the four frontal moraines of the Stetten stadial spread over nearly six kilometres between the towns of Wohlen and Boswil (Fig. 10b). Lateral moraines can be found on the Wagenrain saddle and on the slope of Lindenberg (Fig. 8). Moraines reach >15 m in height and in parts are characterized by sharp crests. This is in strong contrast to the moraine deposits of the LGM maximum stadials further downstream in Bünz Valley. The different appearance of the moraines likely relates to present land use practices where detailed morphological structures are limited primarily to forested areas.

The Bremgarten stadial is built up of two closely spaced and well-preserved moraine sets located ~7.5 km upstream of the outer Stetten stadial moraines in Reuss Valley (Fig. 8). Single frontal and lateral ridges are 15–20 m high. Left lateral moraines of the Bremgarten stadial run continuously over more than ten kilometres along the eastern margin of the Wagenrain Molasse hill, crosscut moraines of the external Stetten stadial, and behead Bünz Valley (Fig. 8, Fig. 10b). The Bremgarten stage is the last recessional stadial preserved on the foreland.

5. Discussion

Building on the geomorphological groundwork introduced in Sections 4.1 and 4.2, new dating results of this study are paired with, carefully reviewed, ages of recent publications in order to construct robust timelines for the LGM phases of Rhine and Reuss glacier systems. All ages considered in the new chronologies are listed with their paleoglaciological context in Table 7 and Table 8. The reconstructed spatial and chronological evolution of Rhine and Reuss glacier systems are discussed in Section 5.1 and 5.2, respectively. Fundamental similarities and differences are pointed out in the last chapter of the discussion.

5.1. *Rhine glacier dynamics during the LGM*

Emerging from the Alpenrhein Valley outlet at Bregenz (Fig. 1) the largely channelized ice stream of the LGM Rhine glacier spread radially outwards along the major foreland overdeepened basins, which mainly follow Lake Constance and Schussen Valley (Fig. 3) (Ellwanger et al.,

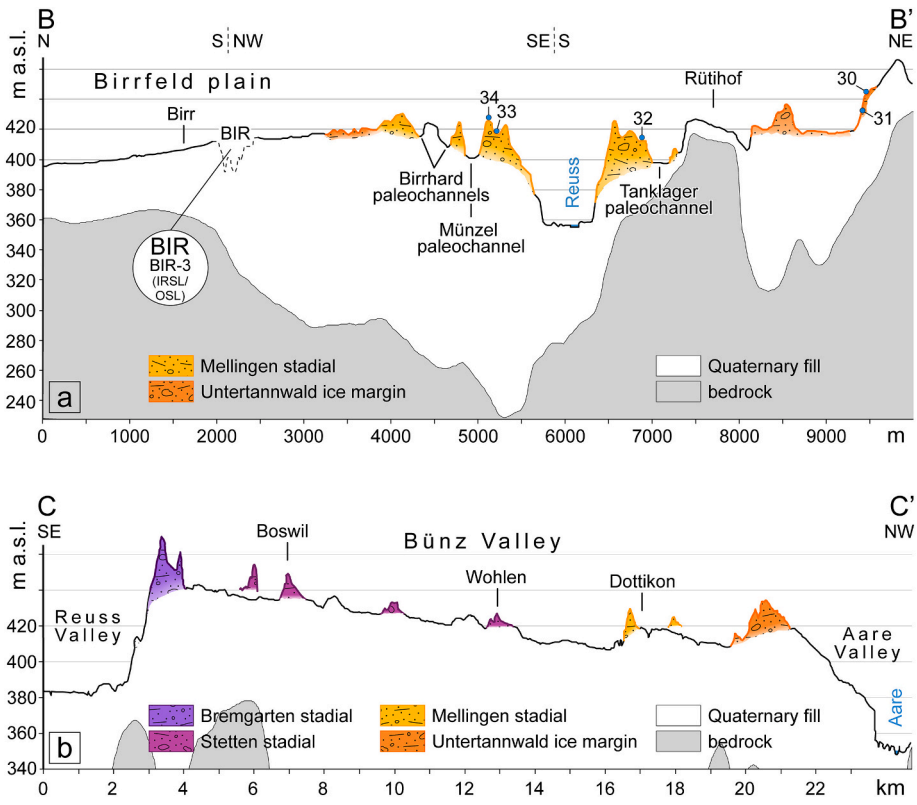

Fig. 10. (a) Cross-section through the Reuss Valley frontal moraine ridges of the LGM maximum (Untertannwald ice margin and Mellingen stadial), and the Birrfeld outwash plain with the 'Joriacher' gravel pit (BIR). The location of the profile is shown in Fig. 8 and Fig. 9. The blue circles indicate the location of exposure dated erratics. The top of a glacial diamicton interbedded with outwash gravels exposed in the BIR gravel pit was OSL and IRSL dated to 25.1 ± 2.4 ka and 24.2 ± 2.2 ka, respectively (Gaar et al., 2019). Vertical exaggeration is approximately 17×; (b) cross-section through Bünz Valley and moraine ridges of the LGM maximum (Untertannwald ice margin, Mellingen moraines), Stetten, and Bremgarten stadials. The location of the profile is shown in Fig. 8. Bremgarten stadial moraines shown are the left lateral moraines of Reuss Valley lobe, whereas all other ridges are frontal moraines of Bünz lobe. Moraine ridges that do not touch the section line are projected in. Vertical exaggeration is approximately 50×. Surface of the bedrock was extracted from the Swiss bedrock elevation model (Federal Office of Topography swisstopo, 2018a). Elevation data provided by the Federal Office of Topography swisstopo.

2011; Keller, 2021). Large volumes of outwash were being deposited in the forefield of the advancing glacier. Outwash was not only directed to the Rhine River but also towards the Danube River with the drainage divide located roughly north of Stockach. Meltwaters of the Argen and Schussen lobes, as well as the eastern parts of the Untersee lobe drained northwards towards the Danube River (Fig. 3). Large parts of the meltwaters emerging from the Thur and Untersee lobes were routed westwards over long distances along the glacier front before draining into Klettgau (Fig. 1, Fig. 3).

Mammoth bones and tusks from three gravel deposits, Markelfingen, Steißlingen (both ^{14}C; this study), and Rafzerfeld (^{14}C, OSL; Preusser et al., 2007), were analysed recently. The Markelfingen gravels (Schreiner, 1968, 1973) are located about twenty kilometres upstream of the outer Schaffhausen stadial moraines (Fig. 3, Fig. 4). Dates from a mammoth tusk found within the Markelfingen gravels (Geyh and Schreiner, 1984) provide a maximum age for the Rhine piedmont lobe reaching its furthest extent during the LGM (Keller and Krayss, 2005a). Our new radiocarbon dates for the Markelfingen tusk yield precise ages that calibrate to 26.4–26.0 ka cal BP and 26.8–26.0 ka cal BP. The presence of an overlying 2–6 m of glacial diamicton with drumlinized morphology, demonstrates that the Rhine glacier advanced over and beyond the Markelfingen site (Fig. 13; Schreiner, 1968; Geyh and Schreiner, 1984; Ellwanger, 1990). Our new radiocarbon ages suggest that the Rhine glacier LGM maximum advance occurred shortly after 26 ka (Fig. 13, Table 7).

Originating from the westernmost part of the Thur lobe, glacial meltwaters drained towards Rafzerfeld plain. Several tens of metres of outwash accumulated when the glacier front was advancing to or located at its maximum position at the eastern end of the Rafzerfeld plain close to Rüdlingen (Fig. 11, Fig. 12; Freimoser and Locher, 1980; Graf, 2009). A sand layer at the top of the Rafz gravels, exposed in the Hüntwangen 'Ghürst' gravel pit (H on Fig. 11 and Fig. 12), was luminescence dated to 25.0 ± 2.0 ka (HÜW1; Preusser et al., 2007). This age is consistent with the radiocarbon date from a mammoth tusk fragment (Wi1: 26.1–25.3 ka cal BP (21,510 ± 160 ^{14}C a BP; ETH-17253); Graf, 2009) found in a gravel pit located just adjacent to the northeast (Wil gravel pit; W on Fig. 11 and Fig. 12; Preusser et al., 2007), where at that time only Rafz gravels were being exploited (Graf, 2009). Two more mammoth bones, a femur (Hü1) and a tibia (Hü2), from the Hüntwangen 'Ghürst' pit were found at ~365 m a.s.l. The bones yielded ^{14}C ages of 22.4–21.9 ka cal BP (18,240 ± 130 ^{14}C a BP; ETH-17254) and 27.0–26.0 ka cal BP (22,190 ± 170 ^{14}C a BP; ETH-17255), respectively (Preusser et al., 2007; Graf, 2009). Very little information on the stratigraphic context is available for these specimen (Graf, 2009). If not reworked, the bones provide markers for the timing of gravel accumulation at the Rafzerfeld outwash plain. OSL and radiocarbon ages from the Rafz gravels are in good agreement with the defined maximum age for the LGM advance derived from our new ^{14}C ages of the Markelfingen tusk (Fig. 13, Table 7).

Before Rhine glacier abandoned its maximum position at the head of Rafzerfeld plain (Rüdlingen ice margin), glacial meltwaters incised the one kilometre wide, nine metre deep Chlainert channel into the outwash plain (Fig. 11, Fig. 12). Small ice blocks were frequently left behind by the withdrawing glacier west of Rüdlingen and at numerous other sections along the piedmont lobe as indicated by kettled and chaotic moraine deposits. With the onset of glacier retreat, the elevated Rafzerfeld plain was cut off from meltwater discharge. As a result, meltwaters bypassed the eastern parts of the Rafzerfeld plain, cut down into the older Rafz gravels (downstream of the town of Eglisau; Fig. 11), and subsequently deposited a few meters of the younger Hüntwangen gravels on the cut terrace surface (Fig. 12; Preusser et al., 2007). The Rafz and Hüntwangen terraces are separated by a ca. 10 m high erosional scarp running from Eglisau to the northwest (Graf, 2009). Two OSL samples (HÜW3, HÜW4) from fine grained sediments within the Hüntwangen gravels, reported by Preusser et al. (2007), indirectly constrain the withdrawal of the Rhine glacier from its maximum position (Table 7). The samples stem from the Hüntwangen 'Ghürst' gravel pit and overlie sample HÜW1 (see above). The ages are 22.2 ± 1.6 ka (HÜW3) and 21.0 ± 1.5 ka (HÜW4; Preusser et al., 2007). The Hüntwangen terrace was carved into the Rafz gravels and the Hüntwangen

Table 7
Rhine glacier chronology. Previously published and newly obtained ages pinning down glacier evolution of the LGM Rhine glacier piedmont lobe on the Swiss-German Alpine foreland in stratigraphic order. Moraine stabilization age shown in bold type. Geological and statistical outliers have been removed. See text for details.

Sequence	Type of evidence	Interpretation	Method	Sample		^{14}C Age BP	Age cal BP	Exposure[a]/luminescence age	Reference
				Name	Material	*a*	*ka*	*ka*	
Lateglacial ice decay Stein am Rhein stadial	Moraine stabilization	Ice free Alpenrhein Valley	^{10}Be	LIE05	Erratic boulder			16.9 ± 0.5 (1.0)	This study
	Moraine formation, sediment sequence	Glacier readvance							Keller and Krayss, 2005b
									Ellwanger et al., 2011
Schaffhausen stadial	Moraine stabilization	Active glacier recession	^{10}Be	RH08	Erratic boulder			17.9 ± 0.6 (1.1)	This study
			^{10}Be	RH07	Erratic boulder			18.7 ± 0.7 (1.2)	This study
			^{10}Be	RH09	erratic boulder			**20.6 ± 1.7 (2.0)**	this study
	Proglacial gravel accumulation	Retreat from LGM maximum position	OSL	HÜW4	Sediment			21.0 ± 1.5	Preusser et al., 2007
			OSL	HÜW3	Sediment			22.2 ± 1.6	Preusser et al., 2007
	Proglacial gravel accumulation	Stabilization at LGM maximum position	^{14}C	Hü1	Mammoth bone	18,240 ± 130	22.4–21.9		Preusser et al., 2007
			OSL	HÜW1	Sediment			25.0 ± 2.0	Preusser et al., 2007
			^{14}C	Wi1	Mammoth tusk	21,510 ± 160	26.1–25.3		Preusser et al., 2007
			^{14}C	Hü2	Mammoth bone	22,190 ± 170	27.0–26.0		Preusser et al., 2007
	Proglacial gravel accumulation	LGM maximum glacier advance	^{14}C	RH-MT-Mkf-1	mammoth tusk	22,125 ± 73	26.8–26.0		This study
				RH-MT-Mkf-2		22,002 ± 72	26.4–26.0		This study

[a] External uncertainties in brackets.

gravels were deposited after Rhine River had relocated to its current channel north of Irchel, thus after the Rhine glacier had abandoned the maximum position at Rüdlingen. Overall, Rhine glacier advanced to and reached its western LGM maximum position between 26 and 22 ka (Fig. 13, Table 7).

During its LGM maximum, Rhine glacier built up chains of moraine ridges that form the prominent outer Schaffhausen ice margin, pointing to a prolonged period of oscillation. Between Engen and Schaffhausen moraine deposits of the LGM maximum were presumably destroyed by channelled meltwaters emanating from the Thur and Untersee lobes. Elsewhere, the morphological character of the frontal moraines changes frequently from chaotic and kettled terrain to more distinct and continuous ridges. These small-scale morphological differences suggest varying proportions of debris across the surface of the LGM glacier terminus. Numerous erratic boulders must have thereby been transported to and deposited at the glacier margins, but are today largely decimated.

The altitude of the ice surface of the LGM glacier during the Schaffhausen stadial can be estimated from the elevations of the frontal moraines and the lateral moraines along the suture zone between the Schussen and Argen lobes. At the margin of the Untersee lobe, the ice surface reached around 660 m a.s.l. This is indicated by glacial deposits on the south slope of Hohenstoffeln (Fig. 4). Based on the suture zone moraines, an ice surface height of minimum 770 m a.s.l. is proposed ten kilometres upstream from the LGM glacier front. The ice surface clearly exceeded ~700 m a.s.l. (north of Stein am Rhein) to ~720 m a.s.l. (north of Markelfingen), as deduced from the elevation of interpreted LGM till overlying Deckenschotter (Graf and Burkhalter, 2016) and other pre-LGM deposits and bedrock (cf. Schreiner, 1992a; Keller and Krayss, 2005b; Bini et al., 2009).

Frequent oscillations of single lobes characterized the pullback of the Rhine glacier from its LGM maximum position. Interim stabilizations led to deposition of multiple indistinct moraines in a belt just upstream from the outer Schaffhausen frontal moraines (Fig. 3, Fig. 13). Across the piedmont lobe, active retreat positions are difficult to decipher and there does not seem to be strong geomorphological evidence to address them as stadial(s). Correlation of the numerous moraines would be speculative, underscored by the fact that different authors have correlated them in different ways over the last 100 years (e.g. Penck and Brückner, 1909; Schmidle, 1914; Hantke, 1983; Keller and Krayss, 2000). Cross-cutting relationships at the interlobate moraines of Schussen and Argen lobes (Fig. 6a), already described by Beckenbach et al. (2014), show that the active retreat of single lobes was in detail not uniform across the ice front. A dated erratic boulder (RH09) from the right lateral moraine of the Schussen lobe at the suture to the Argen lobe (Fig. 6a,b), points to moraine stabilization no later than 20.6 ± 1.7 ka (Fig. 13). This age agrees well with the available chronological constraints from Rafzerfeld plain, that suggest that Rhine glacier was already located upstream of the outer Schaffhausen ice margin by that time (Table 7; Preusser et al., 2007). A younger exposure age obtained from an erratic further to the east provides a minimum age for stabilization of a retreat moraine of the Argen lobe (RH07: 18.7 ± 0.7 ka; Fig. 6a).

Rhine glacier retreated a minimum of five to thirteen kilometres relative to its LGM maximum position before ice volume increased and it readvanced to the Stein am Rhein position. Sedimentological observation from numerous outcrops underline this sequence of events (Schindler et al., 1978; Schreiner, 1992a; Keller and Krayss, 2005b; Ellwanger et al., 2011). The Stein am Rhein stadial is of particular interest as it is the only ice margin upstream of the outer Schaffhausen moraines that can be straightforwardly reconstructed across the whole width of the former piedmont lobe (cf. Penck and Brückner, 1909; Ellwanger et al., 2011; Regierungspräsidium Freiburg, Landesamt für Geologie, Rohstoffe und Bergbau, 2013). Numerous ridges spanning over several kilometres were built up during frequent ice front oscillations associated with the Stein am Rhein stadial. Minimum ice surface elevations of ~650 and 550 m a.s.l. for Thur and Untersee lobes were derived from

Table 8
Reuss glacier chronology. Previously published and newly obtained ages pinning down LGM glacier evolution of the eastern lobe of the Reuss glacier system on the Swiss foreland in stratigraphic order. Moraine stabilization ages shown in bold type. Geological and statistical outliers have been removed. See text for details.

Sequence	Type of evidence	Interpretation	Method	Sample		^{14}C Age BP	Age cal BP	Exposure[a]/luminescence age	Reference
				Name	Material	*a*	*ka*	*ka*	
Deglaciation	Lake sedimentation	Ice free foreland	^{14}C	C823	Terrestrial Macrofossils	14,570 ± 240	**18.3–17.1**		Lotter, 1988 Zbinden et al., 1989
Bremgarten stadial	Moraine formation, cross-cutting relationships	Glacier readvance							this study
Stetten stadial	Moraine stabilization	Active glacier fluctuations	^{10}Be	Reuss-20	Erratic boulder			18.6 ± 0.9 (1.3)	Reber et al., 2014
			^{10}Be	Reuss39	Erratic boulder			**20.8 ± 1.3 (1.7)**	This study
Mellingen stadial	Moraine stabilization	Active glacier fluctuations	^{10}Be	Reuss38	Erratic boulder			17.7 ± 1.0 (1.3)	This study
			^{10}Be	Reuss34	Erratic boulder			18.6 ± 0.8 (1.2)	This study
			^{10}Be	Reuss35	Erratic boulder			19.1 ± 0.8 (1.2)	This study
			^{10}Be	Reuss44	Erratic boulder			20.0 ± 1.6 (1.8)	This study
			^{10}Be	Reuss36	Erratic boulder			20.5 ± 0.8 (1.3)	This study
			^{10}Be	Reuss32	Erratic boulder			**21.1 ± 1.0 (1.4)**	This study
Untertannwald ice margin	Erratic boulder stabilization	Ice surface lowering (Wagenrain)	^{10}Be	Reuss42	Erratic boulder			17.2 ± 1.0 (1.3)	This study
			^{10}Be	Reuss41	Erratic boulder			17.4 ± 1.0 (1.3)	This study
			^{36}Cl	Reuss43	Erratic boulder			19.0 ± 1.8 (2.6)	This study
			^{10}Be	Reuss40	Erratic boulder			**20.3 ± 1.3 (1.6)**	This study
	Moraine stabilization	Active glacier fluctuations	^{10}Be	Reuss30	Erratic boulder			21.2 ± 0.9 (1.4)	This study
			^{10}Be	Reuss46	Erratic boulder			21.7 ± 1.2 (1.6)	This study
			^{10}Be	Reuss-21	Erratic boulder			22.0 ± 0.9 (1.4)	Reber et al., 2014
			^{10}Be	Reuss-22	Erratic boulder			**22.2 ± 1.0 (1.5)**	Reber et al., 2014
	Subglacial till deposition		IRSL	BIR-3	Sediment			24.2 ± 2.2	Gaar et al., 2019
			OSL	BIR-3				25.1 ± 2.4	Gaar et al., 2019

[a] External uncertainties in brackets.

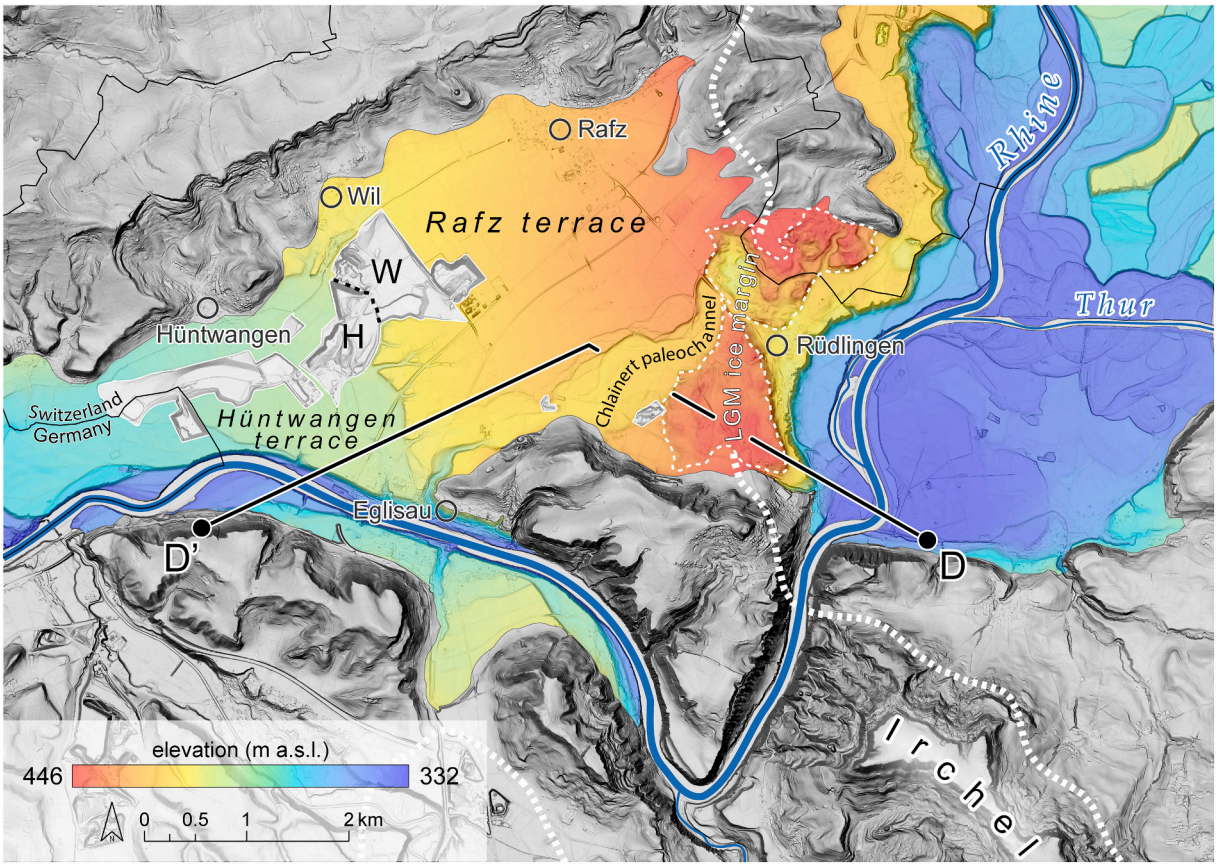

Fig. 11. Rafzerfeld outwash plain in front of the westernmost LGM maximum ice margin (Schaffhausen stadial) of Rhine glacier's Thur lobe at Rüdlingen (Fig. 3, Fig. 15). Locations of the Wil (W) and Hüntwangen 'Ghürst' (H) gravel pits are indicated. A ~ 10 m high erosional scarp separates both gravel pits (black dashed line) and the higher Rafz from the lower Hüntwangen terrace. OSL and radiocarbon ages from the gravel pits of Wil and Hüntwangen (Preusser et al., 2007) provide key evidence for the chronological constraints of the LGM maximum of the Rhine glacier (Fig. 12, Fig. 13, Table 7). White dashed line shows the extent of the LGM maximum glaciation after Bini et al. (2009). Indicated cross-section (D-D′) is shown in Fig. 12. Elevation data provided by the Federal Office of Topography swisstopo.

lateral moraine deposits along isolated bedrock highs north of Frauenfeld and north of Markelfingen (Fig. 3), respectively. At the upstream end of the suture between Schussen and Argen lobes, ice levels during the readvance may have been in the range of 680 m a.s.l. Exposure ages gained in a position external to the Stein am Rhein ice margins restrict the formation of corresponding moraines and the glacier readvance to have occurred after 20.6 ± 1.7 ka (Fig. 13). The Stein am Rhein ice margins possibly represent the last active stabilization of the LGM Rhine glacier on the foreland. Meltback from the Stein am Rhein stadial could have been relatively fast and possibly uninterrupted by significant stabilization phases as only few and scattered moraine ridges are present upstream (Fig. 3). In front of the retreating glacier, ice dammed lakes formed along valley troughs as meltwaters were blocked downstream by adverse slopes or moraine ridges (e.g. Geiger, 1943; Weidenbach, 1975; Schmidt, 1976; Keller and Krayss, 2000).

Final downwasting of the Rhine glacier likely occurred in concert with other major Alpine valleys (van Husen, 1997; Klasen et al., 2007; Schlüchter et al., 2021) in the early Lateglacial phase of ice decay (Reitner, 2007). Stagnant, climatically decoupled, ice bodies may have persisted in the Alpenrhein Valley, but no clear ice marginal landforms were left behind neither at Eschnerberg nor along Fläscher Berg (Fig. 7). We interpret the dated erratics at Eschnerberg to have been let down during retreat or thinning of the glacier rather than during a distinct phase of glacier stabilization. The deglaciation of the lower Alpenrhein Valley likely took place prior to 16.9 ± 0.5 ka (Fig. 13, Table 7) as indicated by exposure ages from Eschnerberg (LIE05; 110–80 km behind the LGM maximum position). Boulder stabilization or exhumation can however be an issue at this site, as indicated by a nearby erratic dated several hundred years younger. We interpret the ages from the upstream site at Fläscher Berg (LIE02: 14.7 ± 0.6 ka, LIE03: 14.2 ± 0.6 ka) to have been strongly affected by exhumation or toppling. Both boulders were located on a steep slope. Sedimentological, paleobotanical, and glacial records from across the Alps document ice-free conditions at the beginning of the Bølling warm phase (14.6 ka; Heiri and Millet, 2005; Samartin et al., 2012; Heiri et al., 2014) not only in the main and tributary valleys (van Husen, 1997; Ivy-Ochs et al., 2009; Heiri et al., 2014; Wirsig et al., 2016) but also of major Alpine passes (Kelly et al., 2006; Dielforder and Hetzel, 2014; Hippe et al., 2014; Scapozza et al., 2014).

5.2. *Reuss glacier dynamics during the LGM*

Outflowing its accumulation areas in central Switzerland, lobes of the LGM Reuss glacier system followed glacially overdeepened valleys on the Swiss forelands (Jordan, 2010; Pietsch and Jordan, 2014). Constrained by topography, ice masses subdivided into narrow individual finger-like lobes (Fig. 8; Bini et al., 2009). During the LGM, single lobes were shallowly connected across the NNW-SSE trending Molasse bedrock highs (Bini et al., 2009) that separate individual valley troughs and are partially covered by pre-LGM gravel deposits (Jäckli, 1966; Gerber and Kopp, 1990; Graf et al., 2007, 2012; Jordan et al., 2011; Gubler, 2020b).

Low-relief frontal moraines provide distinct geomorphological evidence for LGM glacier stabilization of Reuss and Bünz lobes at the Untertannwald ice margin (Fig. 8). Interpreted glacial sediments are

reported from quarries located just external to these moraines (Bitterli-Dreher et al., 2007; Graf, 2009) (Fig. 8, Fig. 9). A sample from the top of an 80 cm thick glacial diamicton, interbedded with outwash gravels and presently exposed at ~5 m depth in a gravel pit on Birrfeld plain (Fig. 10a) was recently assigned to LGM age by means of OSL (25.1 ± 2.4 ka) and IRSL (24.2 ± 2.2 ka) dating (Gaar et al., 2019). Erratic boulders observed in excavation pits and forests of Birmenstorf and around Dättwil are thought to have been deposited coevally (Bitterli-Dreher et al., 2007; Bini et al., 2009; Graf, 2009). Most of the latter are not in original position and have therefore not been dated in this study. In the absence of corresponding frontal or lateral ice marginal landforms and considering the minor thickness of the dated glacial diamicton (Gaar et al., 2019), the till likely formed during a short-lived advance onto downstream outwash plains around 25/24 ± 2 ka while the glacier oscillated at the close-by Untertannwald ice margin (Fig. 14, Table 8). The Untertannwald low-relief ice margin was abandoned no later than 22 ± 1 ka as suggested by several exposure ages from this ice margin (this study; Reber et al., 2014; Table 8).

During its LGM maximum, Reuss lobe reached a minimum ice surface height of ~540 m a.s.l. along the western slope of Heitersberg and ice from the Reuss lobe overflowed across the Wagenrain ridge into the slightly elevated Bünz Valley (Fig. 8). If LGM Bünz and Reuss lobes merged into a ten kilometre wide lobe (Fig. 1; Bini et al., 2009) or stayed separated in close proximity to each other (Jäckli, 1962, 1966) cannot be determined based on geomorphological observations. Whether or not the top of Wagenrain bedrock ridge (Fig. 8) was covered by ice (Jäckli, 1962, 1966; Bini et al., 2009) seems crucial in this regard. New surface exposure samples from the northern part of the Wagenrain ridge were dated to 20.3 ± 1.3 ka, 17.4 ± 1.0 ka, 17.2 ± 1.0 ka, and 19.0 ± 1.8 ka (Reuss40–43). Obtained ages testify to LGM ice surface elevation of at least 540–510 m a.s.l. These results match ice altitudes we reconstructed for the right side of Reuss Valley. With these constraints, if at all, only the highest parts of the Wagenrain plateau (~590 m a.s.l.) would have protruded from the ice during LGM maximum ice extent.

At the glacier front, meltwater streams drained northwards onto the large outwash plains of Birrfeld and Lindenstaldenzelg towards Brugg and along the present-day Reuss Valley. Meltwaters from Bünz lobe flowed across the Lind and Birch plains towards Wildegg (Fig. 8, Fig. 9; Bini et al., 2009; Graf, 2009). Radiocarbon ages from bone samples found in outwash deposits located a few kilometres downstream along Reuss River (Fig. 8) indicate ongoing deposition of gravels at 25.9–25.2 ka cal BP (Ge1: 21,230 ± 160 ^{14}C a BP; ETH-17252; Graf, 2009) and 22.4–21.5 ka cal BP (Tu2: 18,150 ± 140 ^{14}C a BP; ETH-17256; Graf, 2009). These radiocarbon ages are consistent with luminescence ages from Birrfeld plain (Gaar et al., 2019) and surface exposure ages (this study; Reber et al., 2014).

After ca. 22 ± 1 ka (this study; Reber et al., 2014), the northern part of the Wagenrain Molasse ridge became ice free once the glacier had retreated from the Untertannwald low-relief ice margins (Fig. 8, Table 8). At that time meltwaters from Reuss Valley drained over to Bünz Valley in an ice marginal channel north of Hägglingen. Thereafter two individual glacier tongues existed in Bünz and Reuss valleys as shown by the discrete frontal moraine ridges of Mellingen stadial.

The Mellingen moraine complexes of Reuss and Bünz lobes must have built up during a major stabilization or readvance phase (Fig. 8, Fig. 9, Fig. 13; Graf, 2009). At the town of Mellingen the stacked frontal and lateral moraines with four subparallel ridges suggest that the Reuss lobe was oscillating at this position for a significant period of time (Fig. 14, Table 8). Over the course of the Mellingen stadial, the actively retreating Reuss lobe was continuously narrowing from 3.2 km width down to a width of 2 km as evidenced by the internal Mellingen stadial moraines in Reuss Valley (Fig. 8). A concomitant drop in ice level of about 50–60 m is reconstructed based on the elevation of lateral moraine ridges on the right side of the former Reuss lobe (Fig. 8). Boulder

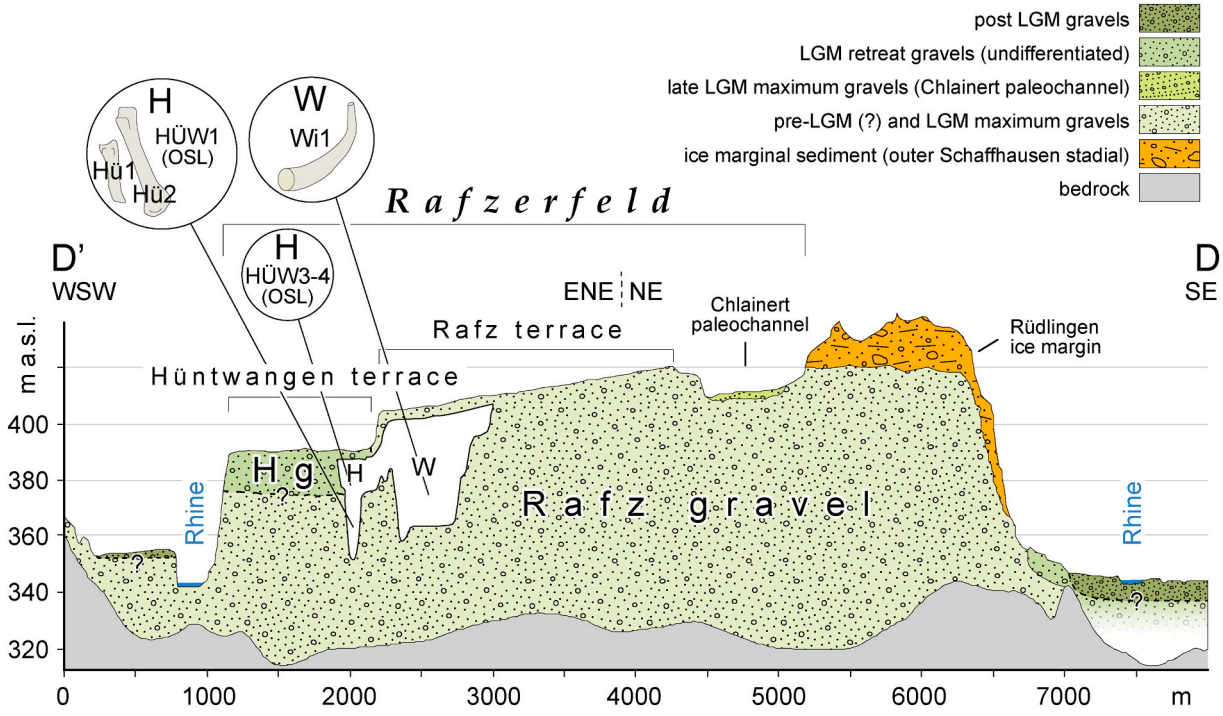

Fig. 12. Cross-section through the outwash deposits of the Rafzerfeld plain and the Rüdlingen ice margin (Schaffhausen stadial) based on work of Freimoser and Locher (1980), Graf (2009), and Preusser et al. (2007). The location of the profile is shown in Fig. 11. Hg: Hüntwangen gravels. Positions of the Wil (W) and Hüntwangen 'Ghürst' (H) gravel pits are projected into the profile. Mammoth tusk (Wi1: 26.1–25.3 ka cal BP) and bones (Hü1: 22.4–21.9 ka cal BP; Hü2: 27.0–26.0 ka cal BP) from Wil and Hüntwangen gravel pits, respectively, were dated by Preusser et al. (2007). An OSL sample (HÜW1) from the Rafz gravels exposed in the Hüntwangen gravel pit was determined to 25.0 ± 2.0 ka (Preusser et al., 2007). OSL samples from the overlying Hüntwangen gravels were dated to 22.2 ± 1.6 ka (HÜW3) and 21.0 ± 1.5 ka (HÜW4; Preusser et al., 2007). Vertical exaggeration is approximately 20×. Surface of the bedrock extracted from the Swiss bedrock elevation model (Federal Office of Topography swisstopo, 2018a). Elevation data provided by the Federal Office of Topography swisstopo.

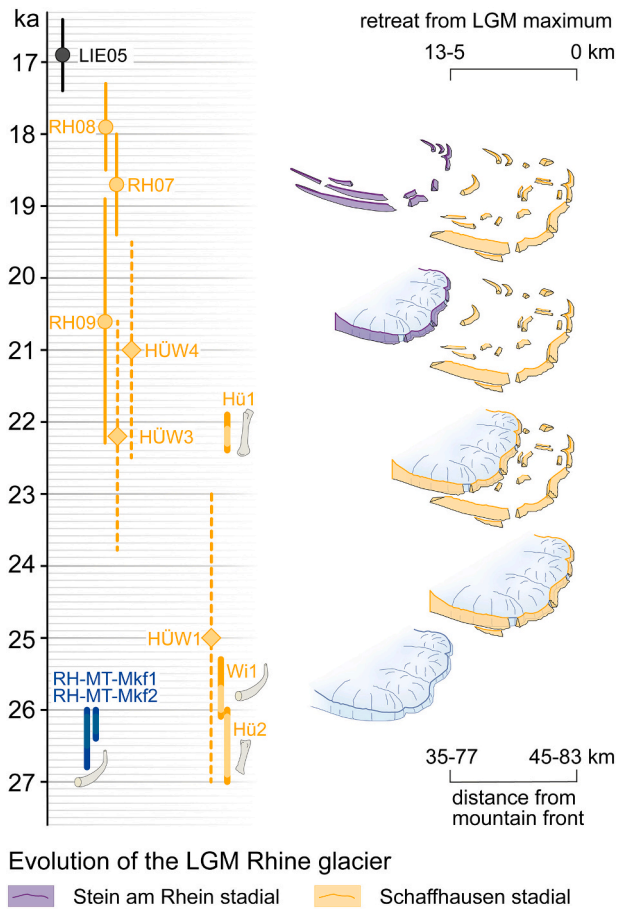

Fig. 13. Schematic ice margin with LGM timing of the Rhine piedmont glacier (see also Table 7). Compilation of recently determined bone radiocarbon (bars with confidence levels of 68.3 % and 95.4 %: Hü1, Hü2, Wi1 (Preusser et al., 2007); RH-MT-Mkf1, RH-MT-Mkf2 (this study)), OSL (dashed lines: HÜW1,3,4 (Preusser et al., 2007)), and surface exposure dates (solid lines: RH07–09, LIE05 (this study)), constraining the evolution of the LGM Rhine glacier on the Swiss-German foreland. Radiocarbon ages from the Markelfingen tusk (blue bars, RH-MT-Mkf1, RH-MT-Mkf2) constrain the deposition of advance gravels in the course of the glacier's advance to the LGM maximum position. Radiocarbon and OSL dated gravels at Rafzerfeld likely encompass both advance to and reaching of the Rüdlingen ice margin (Fig. 11, Fig. 12). Surface exposure age of LIE05 provides a minimum age for the retreat of Rhine glacier into Alpenrhein Valley. Statistical and geological outliers have been removed. See text for details.

exposure ages suggest stabilization of the inner frontal moraines of Mellingen to have occurred around 21.1 ± 1.0 ka (Reuss32). Slightly younger exposure ages (Reuss36: 20.5 ± 0.8 ka; Reuss44: 20.0 ± 1.6 ka) were obtained from outer left and right lateral moraines of the Mellingen stadial. The glacier's retreat from the Mellingen position was possibly underway by then as indicated by the exposure age (Reuss39: 20.8 ± 1.3 ka) gained for the subsequent inner Stetten stadial (Fig. 14).

When the Reuss glacier lobe resided at the outer Mellingen moraines, parts of the meltwaters likely still drained across the Birrfeld plain (Fig. 9). This is indicated by a terrace scarp southwest of Birrhard that cuts through both the Untertannwald low-relief ridges and the outer Mellingen moraines (Fig. 9). Several authors suggested that immense amounts of outwash gravels were emanating from the glacier while it resided at the Mellingen stadial (e.g. Mühlberg, 1905; Penck and Brückner, 1909; Jäckli, 1966), pointing to a significant period of quasi stabilization. It might have been during this phase that the low-relief moraines of the Untertannwald ice margin slightly outboard were partially buried (Mühlberg, 1905; Penck and Brückner, 1909; Jäckli, 1966). The retreat from the outer Mellingen moraines initiated a distinct shift in meltwater drainage. With the activation of the two Birrhard paleochannels (Fig. 9, Fig. 10a), meltwaters were likely directed straight northwards and no longer to the northwest, solely following what would become the present-day course of Reuss River. Coinciding with the deposition of the intermediate Mellingen moraines and no later than 21 ± 1 ka, Birrfeld plain fell dry. The ~400 m wide breach in the inner frontal Mellingen moraines may correspond to the position of Reuss lobes glacier mouth at that particular time (Fig. 9). The Tanklager paleochannel connecting to this moraine opening has similar elevations as the prominent Münzel paleochannel through which meltwaters originating from the left side of the same ice margin drained. The frontal moraine ridges in the centre, today deeply incised by Reuss River, were possibly still intact (Fig. 9, Fig. 10a). The melt back from the inner Mellingen terminal moraines followed soon after and was likely accompanied by distinct lowering of the drainage level as the Reuss lobe retreated and fell back into its former tongue basin. In the course of glacier retreat, the elevated Münzel and Tanklager ice marginal meltwater channels fell dry (Fig. 9, Fig. 10a). Meltwaters trapped in the basin behind the inner Mellingen frontal moraines possibly breached the prominent ridges at the present-day Reuss channel cut. Over in Bünz Valley, the deep channel with its onset between the Mellingen stadial moraines at Dottikon (Fig. 8), may have been initiated during glacier retreat from the Mellingen position (at Dottikon). It could have been further deepened during the meltback from the outer Stetten stadial at Wohlen, for which a phase of incision is geomorphological evidenced.

The restabilization of Reuss and Bünz lobes during the Stetten stadial likely occurred around 20.8 ± 1.3 ka as indicated by the exposure age of a large erratic within the moraine succession (Reuss39). This glacier halt took place soon after the retreat from the Mellingen position (Fig. 14, Table 8). The glacier experienced frequent, small-scale fluctuations that are recorded in multiple moraines in the valleys as well as along the crest of the Wagenrain bedrock ridge, the point of contact between Bünz and Reuss lobes. The glacier front actively oscillated over two kilometres in Reuss Valley and over seven kilometres in Bünz Valley, implying healthy active ice during retreat. On top of Wagenrain, kettle holes are frequently located between multiple moraine ridges suggesting that dead ice blocks were cut off from the retreating glacier front.

Meltwater activities during the retreat from the Stetten stadial and/or the upstream Bremgarten stadial may have largely eroded the frontal sections of the Stetten moraines in Reuss Valley (Fig. 8). In Bünz Valley, downstream outwash deposits, locked behind the inner Mellingen stadial moraine at Dottikon, may have been eroded during the retreat from the Stetten stadial. Besides this incisional phase, lack of erosional landforms in the upstream reach of Bünz Valley suggests ongoing outwash deposition.

The Bremgarten stadial represents the last stabilization phase of the Reuss lobe on the foreland before retreat behind the Alpine fringe. At this particular time, ice from Reuss Valley apparently barely crossed the southernmost part of the Wagenrain ridge and the ice terminated near Muri (Fig. 8). Downstream, the well-preserved, up to 20 m high left lateral moraines of the Reuss arm cross-cut and blocked the head of Bünz Valley completely. Bünz Valley was thus already ice free by that time. The observed cross-cutting relationships likely show a renewed vitalization of the Reuss lobe during the Bremgarten stadial and are associated with a readvance. No chronological evidence is available for the deposition of the Bremgarten moraines except that it had to have been after 20.8 ± 1.3 ka and the retreat from the Stetten stadial (Fig. 14, Table 8). Downwasting of the Reuss glacier likely led to strong incision along the lower reaches of Reuss River. Elevated above the main valley floor (Fig. 9b), Bünz Valley did not receive meltwaters of the decaying Reuss glacier. Consequently, no evidence of strong incision is found there. Deglaciation of the central Swiss foreland was likely completed by 18.3–17.1 ka cal BP (Fig. 14, Table 8), as suggested by the age of identified terrestrial macrofossils (C823) found in a lake core (RL-305) from Lake Rotsee (Fig. 1; Lotter, 1988; Zbinden et al., 1989).

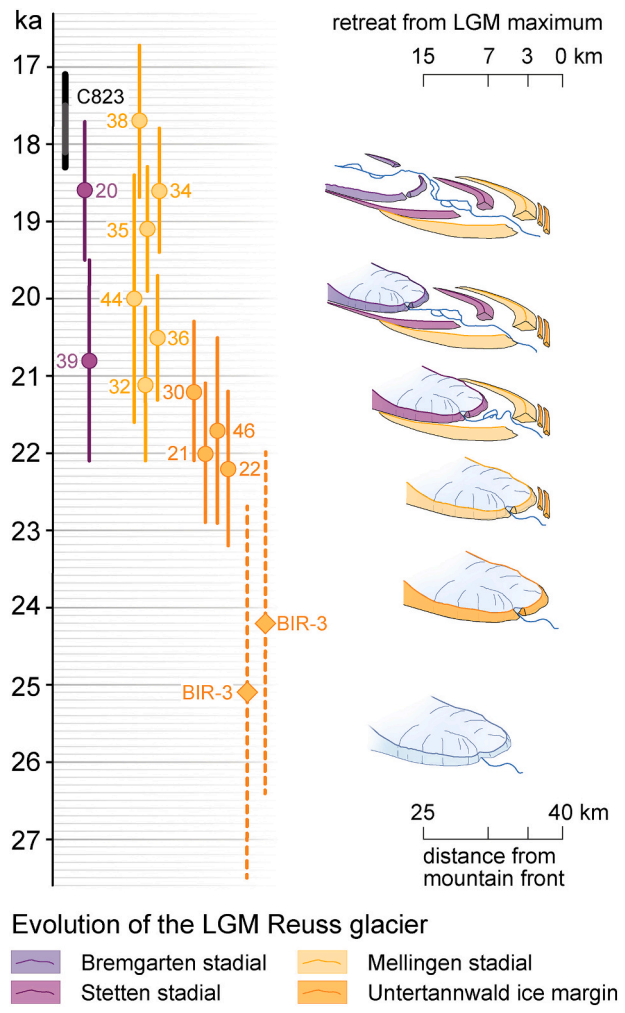

Fig. 14. Schematic ice margin with LGM timing of the Reuss lobe (see also Table 8). Illustrations show the lobe evolution in the Reuss Valley. The LGM maximum corresponds to the low-relief Untertannwald ice margin and the prominent Mellingen stadial. Compilation of radiocarbon (bar with confidence levels of 68.3 % and 95.4 %: C823 (Lotter, 1988; Zbinden et al., 1989)), OSL and IRSL ages (dashed lines: BIR-3 (Gaar et al., 2019)), and surface exposure dates (solid lines: Reuss30–46 (this study), Reuss-20-22 (Reber et al., 2014)) constraining the LGM maximum advances of the Reuss and Bünz glacier lobes on the northern Swiss foreland. Erratic boulder stabilization ages from Wagenrain bedrock ridge are not shown as they do not constrain the frontal position of Reuss glacier. Statistical and geological outliers have been removed. See text for details.

5.3. *Comparing LGM Rhine and Reuss glacier systems on the foreland*

The Rhine and Reuss glacier systems for all their disparities in aerial extent, topographical control, and geomorphological expression show some marked similarities, especially with respect to timing (Fig. 13, Fig. 14, Table 7, Table 8). It is likely that both glaciers had crossed beyond the mountain front and arrived at the forelands by 26–25 ka. In the Rhine glacier this is shown by the Markelfingen ^{14}C dates (this study) and the ^{14}C and OSL dates at Rafzerfeld plain (Preusser et al., 2007). In the eastern Reuss system the LGM maximum extent was reached at ~25/24 ± 2 ka (Gaar et al., 2019) possibly during a short-lived advance while the glacier resided at the nearby Untertannwald ice margin. Oscillation of the huge Rhine glacier piedmont lobe at the outer Schaffhausen ice margin led to the construction of a roughly contiguous system of closely stacked frontal moraines (Fig. 15). This is in contrast to the Reuss system where a two-fold LGM maximum has been recognized (Untertannwald and Mellingen moraines). Abandonment of the outermost Schaffhausen moraines of the Rhine glacier system occurred no later than 22 ka as suggested by a second set of concordant radiocarbon and luminescence ages from the Rafzerfeld site (Preusser et al., 2007). Concurrently, the Reuss glacier lobe had already retreated from the Untertannwald ice margin by 22 ± 1 ka (this study; Reber et al., 2014). Stacked moraines of the Mellingen stadial, dated to 21 ± 1 ka, were built up very soon after. Largely in phase with the pull back of the Reuss lobe, a Schaffhausen stadial recessional moraine of Rhine glacier was exposure dated to have stabilized no later than 20.6 ± 1.7 ka.

Upstream of the LGM maximum moraines, numerous moraine ridges on the foreland of Rhine and Reuss glacier systems highlight the actively oscillating character of both ice fronts. In the Reuss glacier system, internal ice marginal deposits are assigned to two stadials: Stetten and Bremgarten stadials (Fig. 15). With the Stein am Rhein moraine complex, only one major internal LGM position was reconstructed for the Rhine glacier. Nevertheless, in parts of the Rhine glacier system, the outer ridges of the Stein am Rhein moraine complex may loosely correspond to the Stetten stadial of the Reuss system (e.g. around Andelfingen or south of Kißlegg; Fig. 15), as suggested in previous studies (Keller and Krayss, 2005b). Definitive correlation of the Reuss Valley Stetten stadial across the whole of the Rhine piedmont lobe seems speculative, again likely as a consequence of the broad and complex series of ridges. Sedimentological evidence shows that the Stein am Rhein ice margins of the Rhine glacier built up during a glacier readvance (Schreiner, 1973; Schindler et al., 1978; Keller and Krayss, 1987, 2005b; Ellwanger et al., 2011; Fiebig et al., 2011). Readvance character of the Bremgarten stadial is likewise shown by the clear moraine cross-cutting relationships on the left side of Reuss Valley (left lateral moraines just east of Muri; Fig. 8, Fig. 10b). While no direct ages are available from these ice margins, the maximum age for the readvance of Reuss lobe and Rhine glacier are constrained to have occurred after 20.8 ± 1.3 ka and 20.6 ± 1.7 ka, respectively (Table 7, Table 8). Both geomorphologically and chronologically, the Stein am Rhein stadial can be correlated to the Bremgarten stadial (Fig. 15). The narrow, laterally confined Reuss glacier lobes may have reacted more readily and advanced with climatically forced increases in mass balance, constructing numerous easy to distinguish moraine sets. This is in contrast to the perhaps less sensitive Rhine piedmont glacier lobe, which may have had greater inertia.

Moraine ridges of the described readvance stadials reflect the last morphologically well-constrained foreland positions of Rhine and Reuss glaciers (Fig. 15). The rapid collapse of both foreland glaciers likely occurred without significant glacier halts as upstream moraines are lacking (Schlüchter, 1988; Reitner, 2007). Several ^{14}C dates indicate an ice-free Swiss foreland no later than 18 ka (Rey et al., 2020 and references therein).

6. Conclusions

Geomorphological mapping based on high-resolution elevation data combined with field survey allows detailed delineation of conserved relicts of past foreland glaciations. Paired with critically assessed surface exposure, luminescence, and radiocarbon ages of this and previous studies, mapping of past ice margins provides insights into the spatial and chronological evolution of Reuss and Rhine glaciers during the LGM. Our study emphasizes the importance of combining different dating methods with a profound geomorphological understanding when establishing paleoglacier chronologies.

The large Alpine accumulation area and the distinct flow path along Alpenrhein Valley and pre-existing foreland basins and troughs led to the organization of Rhine glacier ice into a large piedmont lobe with a semi-circular footprint, whose LGM maximum extent is clearly defined by a prominent frontal moraine complex (Schaffhausen stadial). Single lobes are well-mimicked by a string of terminal moraines, but preservation differs strongly across the former ice margin, possibly as a consequence of varying drainage configurations. Our new age of the

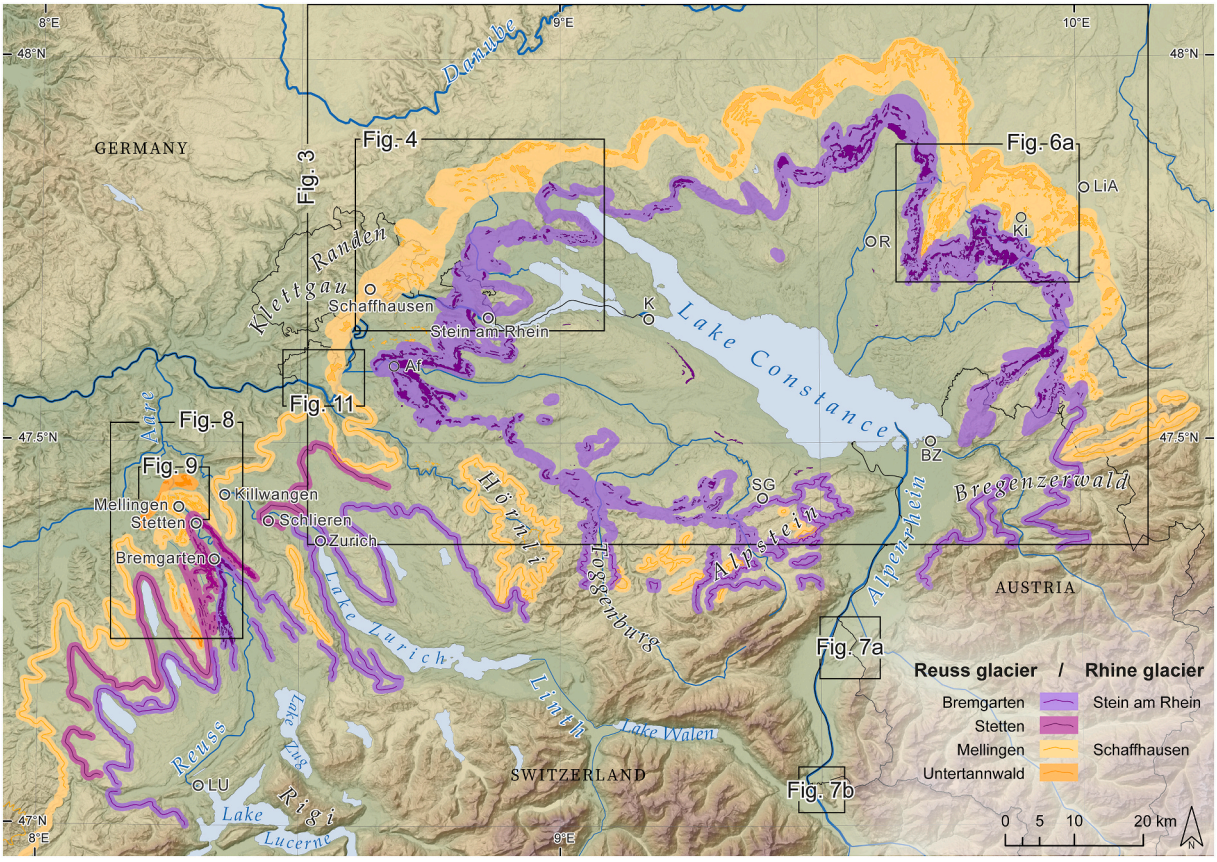

Fig. 15. Ice marginal deposits on the northern Alpine foreland recording LGM glacier fluctuations of the Rhine and Reuss glacier systems. Moraine deposits and stadial configurations of the Rhine glacier piedmont lobe and the eastern Reuss glacier lobe have been mapped in this study. Single ice margins in the Reuss are more readily distinguishable, while distinction of stadials along the extensive front of Rhine glacier is oftentimes ambiguous. The outer ridges of the Stein am Rhein moraine complex may, in parts, loosely correspond to the Stetten stadial of the Reuss system. Glacier extents in the western Reuss lobes and Linth-Rhine glacier lobe (solid line) modified after Hantke (1983), Keller and Krayss (2005b), and Bini et al. (2009). Cities: Af: Andelfingen, BZ: Bregenz, K: Konstanz, Ki: Kißlegg, LiA: Leutkirch im Allgäu, LU: Luzern, R: Ravensburg, SG: St. Gallen. Elevation data provided by European Union, Copernicus Land Monitoring Service 2020, European Environment Agency.

Markelfingen mammoth tusk found in the top section of advance gravels overlain by till, suggests that Rhine glacier advanced to its LGM maximum extent after 26.4–26.0 ka cal BP. Combined with OSL and radiocarbon dates from advance gravels at Rafzerfeld (Preusser et al., 2007), Rhine glacier likely was at its LGM maximum position from ~26–22 ka. A wide band of fragmented recessional moraines lies between the terminal moraines of the LGM maximum and the moraine deposits of the readvance to the Stein am Rhein stadial position. Frontal moraines of the Stein am Rhein ice margin are recognizable over the full width of the piedmont glacier. Due to lack of erratic boulders no direct age constraints for this glacier readvance are available but stabilization ages of moraines just downstream suggest it occurred after 20.6 ± 1.7 ka. Collapse of the foreland lobe likely took place soon after the readvance. The basin of Lake Constance and the lower Alpenrhein Valley were free of ice by no later than 16.9 ± 0.5 ka as indicated by an erratic boulder exposure date at Eschnerberg (105–65 km upstream from Stein am Rhein ice margin).

Upon reaching the central Swiss foreland, ice masses of the Reuss glacier system organized into narrow glacier arms parallel to the elongated Molasse bedrock highs. These topographic constraints resulted in a relatively simple geometry of Bünz and Reuss lobes such that glacier evolution can be readily deciphered from the preserved glacial landforms and deposits. Reuss glacier was oscillating at its maximum position (Untertannwald ice margin) roughly from 25 to 22 ka as suggested from luminescence (Gaar et al., 2019) and surface exposure dates (this study; Reber et al., 2014). Following abandonment of the low-relief Untertannwald ice margin by 22 ± 1 ka, the sharp-crested frontal moraines at Mellingen were constructed. The latter stabilized at ca. 21 ± 1 ka. The deposition of moraines during the upstream Stetten stadial is the result of active glacier retreat. Soon after, the Bremgarten readvance likely occurred not before 20.8 ± 1.3 ka and left behind prominent lateral and frontal moraine ridges. The presence of cross-cutting lateral moraines indicates that by that time, the elevated Bünz Valley was cut off from ice masses and melt waters of the Reuss lobe. Lack of upstream ice margins suggests collapse of the Reuss glacier and retreat behind the mountain front soon after the Bremgarten readvance. Deglaciation of the central Swiss foreland was likely completed no later than 18 ka (Rey et al., 2020).

Despite marked differences in ice volume and morphological expression on the foreland, the Reuss glacier lobes and the Rhine glacier seem to have behaved largely in phase during the LGM. Rhine glacier existed as a broad >100 km wide piedmont lobe, while the lobes of the Reuss glacier system were long and narrow within the parallel valleys on the central Swiss foreland. LGM maximum extents in both systems were reached roughly from 26 to 22 ka. Extensive complexes of stacked frontal moraines were constructed, indicating that both glaciers oscillated at the maximum position for a significant period of time. In the Rhine as well as the Reuss glacier systems active retreat left moraine sets upstream. Sedimentological and geomorphological evidence attests to a clear glacier readvance after 20.8 ± 1.3 ka and 20.6 ± 1.7 ka for Rhine and Reuss glaciers, respectively. Lack of geomorphological evidence of ice margin stabilization suggests subsequent rapid glacier collapse in

both systems.

Declaration of competing interest

The authors declare that they have no known competing financial interests or personal relationships that could have appeared to influence the work reported in this paper.

Data availability

Data will be made available on request.

Acknowledgements

We are grateful to Olivia Steinemann, Ewelina Broś, and Karin Wyss Heeb for their support and counsel in the course of sample preparation. All members of the Ion Beam Physics group, ETH Zurich are thanked for their contributions to the AMS measurements. We appreciate the cooperation with Velten Wagner (Städtisches Museum Engen), Martina Kroth (Bodensee-Naturmuseum, Konstanz), Sabine Kuhlmann (Hegau Museum, Singen), and the Anne-Frank-Schulverbund Engen and the access to the museum and school collections. Jürgen Hald kindly provided the records of Jörg Aufdermauer (Kreisarchäologie Konstanz, 1978). We thank editor Markus Stoffel and two anonymous reviewers for insightful and useful suggestions. This work was carried out in the scope of the doctoral thesis of Sarah Kamleitner and the master thesis of Lucia Manatschal. Funding from the Swiss National Science foundation [SNF grant number 175794, 2017] is gratefully appreciated.

References

Agassiz, L., 1838. Upon glaciers, moraines, and erratic blocks; being the address delivered at the opening of the Helvetic Natural history Society, at Neuchatel, on the 24th of July 1837 by its President. Edinburgh New Philos. J. 24, 364–383.
Akçar, N., Ivy-Ochs, S., Kubik, P.W., Schlüchter, C., 2011. Post-depositional impacts on "Findlinge" (erratic boulders) and their implications for surface-exposure dating. Swiss J. Geosci. 104, 445–453.
Alfimov, V., Ivy-Ochs, S., 2009. How well do we understand production of 36Cl in limestone and dolomite? Quat. Geochronol. 4, 462–474.
André, M.F., 2002. Rates of Postglacial rock weathering on glacially scoured outcrops (Abisko-Riksgränsen area, 68°N). Geogr. Ann. Ser. A Phys. Geogr. 84, 139–150.
Balco, G., Stone, J.O., Lifton, N.A., Dunai, T.J., 2008. A complete and easily accessible means of calculating surface exposure ages or erosion rates from 10Be and 26Al measurements. Quat. Geochronol. 3, 174–195.
Balco, G., Briner, J., Finkel, R.C., Rayburn, J.A., Ridge, J.C., Schaefer, J.M., 2009. Regional beryllium-10 production rate calibration for late-glacial northeastern North America. Quat. Geochronol. 4, 93–107.
Beckenbach, E., Müller, T., Seyfried, H., Simon, T., 2014. Potential of a high-resolution DTM with large spatial coverage for visualization, identification and interpretation of young (Würmian) glacial geomorphology: a case study from Oberschwaben (southern Germany). E&G Quat. Sci. J. 63, 107–129.
Becker, P., Seguinot, J., Jouvet, G., Funk, M., 2016. Last Glacial Maximum precipitation pattern in the Alps inferred from glacier modelling. Geogr. Helv. 71, 173–187.
Beckmann, M., 2004. Pollenanalytische Untersuchung der Zeit der Jäger und Sammler und der ersten Bauern an zwei Lokalitäten des Zentralen Schweizer Mittellandes Umwelt und erste Eingriffe des Menschen in die Vegetation vom Paläolithikum bis zum Jungneolithikum. Dissertationes botanicae 390.
Benz-Meier, C., 2003. Der würmeiszeitliche Rheingletscher - Maximalstand Digitale Rekonstruktion, Modellierung und Analyse mit einem Geographischen Informationssystem. Universität Zürich.
Bini, A., Buoncristiani, J.-F., Couterrand, S., Ellwanger, D., Felber, M., Florineth, D., Graf, H.R., Keller, O., Kelly, M., Schlüchter, C., Schoeneich, P., 2009. Die Schweiz während Des Letzteiszeitlichen Maximums (LGM). Bundesamt für Landestopografie swisstopo, Wabern.
Bitterli-Dreher, P., Graf, H.R., Naef, H., Diebold, P., Matousek, F., Burger, H., Pauli-Gabi, T., 2007. Blatt 1070 Baden. - Geol. Atlas Schweiz 1: 25 000, Erläut, 120. Bundesamt für Landestopografie swisstopo, Wabern.
Borchers, B., Marrero, S., Balco, G., Caffee, M., Goehring, B., Lifton, N., Nishiizumi, K., Phillips, F., Schaefer, J., Stone, J., 2016. Geological calibration of spallation production rates in the CRONUS-Earth project. Quat. Geochronol. 31, 188–198.
Braakhekke, J., Ivy-Ochs, S., Monegato, G., Gianotti, F., Martin, S., Casale, S., Christl, M., 2020. Timing and flow pattern of the Orta Glacier (European Alps) during the last Glacial Maximum. Boreas 49, 315–332.
Briner, J.P., Kaufman, D.S., Manley, W.F., Finkel, R.C., Caffee, M.W., 2005. Cosmogenic exposure dating of late Pleistocene moraine stabilization in Alaska. Bull. Geol. Soc. Am. 117, 1108–1120.
Brock, F., Higham, T., Ramsey, C.B., 2007a. Radiocarbon Dating Bone Samples Recovered from Gravel Sites. In: English Herit. Res. Dept. Rep, Ser, p. 30.
Brock, F., Ramsey, C.B., Higham, T., 2007b. Quality Assurance of Ultrafiltered Bone Dating. Radiocarbon 49, 187–192.
Bronk Ramsey, C., 2009. Bayesian analysis of radiocarbon dates. Radiocarbon 51, 337–360.
Castelletti, L., Livio, F., Martinelli, E., Michetti, A.M., Motella De Carlo, S., 2013. Recenti ricerche paleoecologiche in ambito lariano svolte in collaborazionefra Università dell'Insubria e Laboratorio di archeobiologia Dei Musei Civici di Como. Riv. archeol. dell'antica Prov. e Diocesi di Como 195, 115–128.
Chaline, J., Jerz, H., 1984. Arbeitsergebnisse der Subkommission für Europäische Quartärstratigraphie. Stratotypen des Würm-Glazials. Eiszeitalter und Gegenwart 35, 185–206.
Christl, M., Vockenhuber, C., Kubik, P.W., Wacker, L., Lachner, J., Alfimov, V., Synal, H. A., 2013. The ETH Zurich AMS facilities: Performance parameters and reference materials. Nucl. Instruments Methods Phys. Res. SectB Beam Interact. with Mater. Atoms 294, 29–38.
Claude, A., Ivy-Ochs, S., Kober, F., Antognini, M., Salcher, B., Kubik, P.W., 2014. The Chironico landslide (Valle Leventina, southern Swiss Alps): age and evolution. Swiss J. Geosci. 107, 273–291.
Cohen, D., Gillet-Chaulet, F., Haeberli, W., Machguth, H., Fischer, U.H., 2018. Numerical reconstructions of the flow and basal conditions of the Rhine glacier, European Central Alps, at the last Glacial Maximum. Cryosphere 12, 2515–2544.
Collins, M.J., Nielsen-Marsh, C.M., Hiller, J., Smith, C.I., Roberts, J.P., Prigodich, R.V., Wess, T.J., Csapò, J., Millard, A.R., Turner-Walker, G., 2002. The survival of organic matter in bone: a review. Archaeometry 44, 383–394.
de Charpentier, J., 1835. Notice Sur la cause probable du transport des blocs erratiques de la Suisse. Ann. des Mines 3, 219–236.
de Charpentier, J., 1841. Essai Sur les Glaciers et Sur le Terrain Erratique du Bassin du Rhône. Imprimerie et Librairie de Marc Ducloux, Lausanne.
de Graaff, L.W.S., de Jong, M.G.G., 1995. Notes on the Alpine Rhine glacier and the chronostratigraphy of the Upper Würm. Meded. Rijks Geol. D. 52, 317–330.
de Jong, M.G.G., 1983. Quaternary deposits and landforms of western Allgau (Germany) and the deglaciation after the last major Pleistocene ice advance. Publ. - Fys. Geogr. en Bodemkd. Lab. van Univ. van Amsterdam 36.
de Quervain, F., 1962. Der Stein in der Baugeschichte Zürichs. Vierteljahrsschr. Nat. forsch. Ges. Zür. 107, 1–16.
Del Gobbo, C., Colucci, R.R., Monegato, G., Žebre, M., Giorgi, F., 2022. Atmosphere-cryosphere interactions at 21 ka BP in the European Alps. Clim. Past. https://doi.org/10.5194/cp-2022-43. Preprint.
Diebold, P., Bitterli-Brunner, P., Naef, H., 2005. Blatt 1069/1049 Frick-Laufenburg. – Geol. Atlas Schweiz 1: 25 000, Karte 110. Bundesamt für Landestopografie swisstopo, Wabern.
Dielforder, A., Hetzel, R., 2014. The deglaciation history of the Simplon region (southern Swiss Alps) constrained by 10Be exposure dating of ice-molded bedrock surfaces. Quat. Sci. Rev. 84, 26–38.
Dunai, T.J., 2010. Cosmogenic nuclides. In: Principles, Concepts and Applications in the Earth Surface Sciences. Cambridge University Press, Cambridge.
Ellwanger, D., 1990. Würmzeitliche Drumlinformung bei Markelfingen (westlicher Bodensee, Baden-Württemberg). In: Jahresberichte und Mitteilungen des Oberrheinischen Geol, 72. Vereins, pp. 411–434.
Ellwanger, D., 1992. Lithology and stratigraphy of some Rhine glacier drumlins (South German Alpine Foreland). Geomorphology 6, 79–88.
Ellwanger, D., Wielandt-Schuster, U., Franz, M., Simon, T., 2011. The Quaternary of the southwest German Alpine Foreland (Bodensee-Oberschwaben, Baden-Württemberg, Southwest Germany). E&G Quat. Sci. J. 60, 306–328.
Eugster, H., Fröhlicher, H., Saxer, F., 1960. Geologischer Atlas der Schweiz 1: 25 000 Blatt st. Gallen - Appenzell. Kümmerly & Frey AG, Bern.
Eugster, H., Forrer, M., Fröhlicher, H., Kempf, T., Schlatter, L., Blaser, R., Funk, H., Langenegger, H., Spoerri, M., Habicht, K., 1982. Blatt 1115 Säntis. - Geol. Atlas Schweiz 1: 25 000, Karte 78. Bundesamt für Landestopografie swisstopo, Wabern.
Evans, J.M., Stone, J.O.H., Fifield, L.K., Cresswell, R.G., 1997. Cosmogenic chlorine-36 production in K-feldspar. Nucl. Instruments Methods Phys. Res. SectB Beam Interact. with Mater. Atoms 123, 334–340.
Federal Office of Meteorology and Climatology MeteoSwiss, 2016. Data portal IDAweb. https://www.meteoswiss.admin.ch/home/services-and-publications/beratung-und-service/datenportal-fuer-experten.html. (Accessed 22 September 2021).
Federal Office of Topography swisstopo, 2018. Felsoberflächenmodell (TopFels25).
Federal Office of Topography swisstopo, 2018. swissALTI3D. Das hoch aufgelöste Terrainmodell der Schweiz.
Federici, P.R., Ribolini, A., Spagnolo, M., 2017. Glacial history of the Maritime Alps from the last Glacial Maximum to the Little Ice Age. Geol. Soc. Spec. Publ. 433, 137–159.
Fiebig, M., Ellwanger, D., Doppler, G., 2011. Pleistocene glaciations of southern Germany. In: Ehlers, J., Gibbard, P.L., Hughes, P.D. (Eds.), Quaternary Glaciations - Extent and Chronology. A Closer Look. Elsevier Inc., Oxford, pp. 163–173.
Fink, D., Vogt, S., Hotchkis, M., 2000. Cross-sections for 36Cl from Ti at Ep = 35–150 MeV: applications to in-situ exposure dating. Nucl. Instruments Methods Phys. Res. SectB Beam Interact. with Mater. Atoms 172, 861–866.
Florineth, D., Schlüchter, C., 1998. Reconstructing the last Glacial Maximum (LGM) ice surface geometry and flowlines in the Central Swiss Alps. Eclogae Geol. Helv. 91, 391–407.
Freimoser, M., Locher, T., 1980. Gedanken zur pleistozänen Landschaftsgeschichte im nördlichen Teil des Kantons Zürich aufgrund hydrogeologischer Untersuchungen. Eclogae Geol. Helv. 73, 251–270.

Gaar, D., Lowick, S.E., Preusser, F., 2014. Performance of different luminescence approaches for the dating of known-age glaciofluvial deposits from northern Switzerland. Geochronometria 41, 65–80.
Gaar, D., Graf, H.R., Preusser, F., 2019. New chronological constraints on the timing of late Pleistocene glacier advances in northern Switzerland. Quat. Sci. J. 68, 53–73.
Geiger, E., 1943. Geologischer Atlas der Schweiz 1: 25 000 Blätter: 56 Pfyn, 57 Märstetten, 58 Frauenfeld, 59 Bussnang. Kümmerly & Frey AG, Bern.
Geiger, E., 1968. Geologischer Atlas der Schweiz 1: 25 000 Blatt 1054 Weinfelden. Wassermann AG, Basel.
GeoMol Team, 2015. GeoMol– Assessing Subsurface Potentials of the Alpine Foreland Basins for SustainablePlanning and Use of Natural Resources – Project Report. Augsburg.
Gerber, M.E., Kopp, J., 1990. Geologischer Atlas der Schweiz 1: 25 000. 1129 Sursee Erläuterungen. Bundesamt für Landestopographie, Wabern, Blatt.
German, R., Mader, M., 1976. Die Äußere Jugendmoräne bei Bad Waldsee und das Riedtal. Jahreshefte der Gesellschaft für Naturkd. Württemb. 131, 39–49.
Geyh, M.A., Schreiner, A., 1984. 14C-datierungen an Knochen- und Stoßzahnfragmenten aus würmzeitlichen Ablagerungen im westlichen Rheingletschergebiet (Baden-Württemberg). Eiszeit. Gegenw. 34, 155–161.
Gianotti, F., Forno, M.G., Ivy-Ochs, S., Monegato, G., Pini, R., Ravazzi, C., 2015. Stratigraphy of the Ivrea morainic amphitheatre (NW Italy): an updated synthesis. Alp. Mediterr. Quat. 28, 29–58.
Gosse, J.C., Phillips, F.M., 2001. Terrestrial in situ cosmogenic nuclides: Theory and application. Quat. Sci. Rev. 20, 1475–1560.
Graf, A., Akçar, N., Ivy-Ochs, S., Strasky, S., Kubik, P.W., Christl, M., Burkhard, M., Wieler, R., Schlüchter, C., 2015. Multiple advances of Alpine glaciers into the Jura Mountains in the Northwestern Switzerland. Swiss J. Geosci. 108, 225–238.
Graf, H.R., 2009. Stratigraphie von Mittel- und Spätpleistozän in der Nordschweiz. In: Beiträge zur Geologischen Karte der Schweiz (N. F.). Landesgeologie, swisstopo, Wabern.
Graf, H.R., Bitterli-Dreher, P., Burger, H., Bitterli, T., Diebold, P., Naef, H., 2007. Blatt 1070 Baden (mit Beiträgen von R. Schürch). - Geol. Atlas Schweiz 1: 25 000, Karte 120. Bundesamt für Landestopografie swisstopo, Wabern.
Graf, H.R., Jost, J., Eberhard, M., Kruysse, H., Reber, D., Willenberg, H., 2012. Blatt 1109 Schöftland. - Geol. Atlas Schweiz 1: 25 000, Karte 150. Bundesamt für Landestopografie swisstopo, Wabern.
Graf, H.R., Burkhalter, R., 2016. Quaternary deposits: concept for a stratigraphic classification and nomenclature—an example from northern Switzerland. Swiss J. Geosci. 109, 137–147.
Gribenski, N., Valla, P.G., Preusser, F., Roattino, T., Crouzet, C., Buoncristiani, J.-F., 2021. Out-of-phase late Pleistocene glacial maxima in the Western Alps reflect past changes in North Atlantic atmospheric circulation. Geology 49, 1096–1101.
Groos, A.R., Akçar, N., Yesilyurt, S., Miehe, G., Vockenhuber, C., Veit, H., 2021. Nonuniform late pleistocene glacier fluctuations in tropical Eastern Africa. Sci. Adv. 7, 6826–6838.
Gubler, T., 2020. In: Blatt 1110 Hitzkirch. - Geol. Atlas Schweiz 1: 25 000, Erläut. Bundesamt für Landestopografie swisstopo, Wabern, p. 168.
Gubler, T., 2020. Blatt 1110 Hitzkirch. - Geol. Atlas Schweiz 1: 25 000, Karte 168. Bundesamt für Landestopografie swisstopo, Wabern.
Hajdas, I., Bonani, G., Furrer, H., Mäder, A., Schoch, W., 2007. Radiocarbon chronology of the mammoth site at Niederweningen, Switzerland: results from dating bones, teeth, wood, and peat. Quat. Int. 164–165, 98–105.
Hajdas, I., Michczyński, A., Bonani, G., Wacker, L., Furrer, H., 2009. Dating Bones near the Limit of the Radiocarbon Dating Method: Study Case Mammoth from Niederweningen, ZH Switzerland. Radiocarbon 51, 675–680.
Hajdas, I., Sojc, U., Ivy-Ochs, S., Akçar, N., Deline, P., 2021. Radiocarbon Dating for the Reconstruction of the 1717 CE Triolet Rock Avalanche in the Mont Blanc MassifItaly. Front. Earth Sci. 8, 735.
Haldimann, P., Graf, H.R., Jost, J., 2017. Blatt 1071 Bülach. – Geol. Atlas Schweiz 1: 25 000, Karte 151. Bundesamt für Landestopografie swisstopo, Wabern.
Hantke, R., 1968. Die Diffluenz des würmeiszeitlichen Rheingletschers bei Sargans (Kanton St. Gallen) und die spätglazialen Gletscherstände in der Walensee-Talung und im Rheintal. E&G Quat. Sci. J. 19, 219–226.
Hantke, R., 1983. Eiszeitalter die jüngste Erdgeschichte der Schweiz und ihrer Nachbargebiete. In: Westliche Ostalpen mit ihrem bayerischen Vorland bis zum Inn-Durchbruch und Südalpen zwischen Dolomiten und Mont Blanc, 3rd ed. Ott Verlag, Thun.
Hantke, R., 2003. Blatt 1076 St. Margarethen (Westhälfte) und 1096 Diepoldsau (Westhälfte) mit NW-Ecke von Blatt 1116 Feldkirch. - Geol. Atlas Schweiz 1: 25 000, Karte 108. Bundesamt für Wasser und Geologie, Bern.
Hedges, R.E.M., Law, I.A., 1989. The radiocarbon dating of bone. Appl. Geochem. 4, 249–253.
Heim, A., 1919. Geologie der Schweiz. Tauchnitz, Leipzig.
Heiri, O., Millet, L., 2005. Reconstruction of late Glacial summer temperatures from chironomid assemblages in Lac Lautrey (Jura, France). J. Quat. Sci. 20, 33–44.
Heiri, O., Koinig, K.A., Spötl, C., Barrett, S., Brauer, A., Drescher-Schneider, R., Gaar, D., Ivy-Ochs, S., Kerschner, H., Luetscher, M., Moran, A., Nicolussi, K., Preusser, F., Schmidt, R., Schoeneich, P., Schwörer, C., Sprafke, T., Terhorst, B., Tinner, W., 2014. Palaeoclimate records 60–8 ka in the austrian and Swiss Alps and their forelands. Quat. Sci. Rev. 106, 186–205.
Heissel, W., Oberhauser, R., Schmidegg, O., 1967. Geologische Karte Des Walgaues. Vorarlberg, Geologische Bundesanstalt, Wien.
Heyman, J., Stroeven, A.P., Harbor, J.M., Caffee, M.W., 2011. Too young or too old: evaluating cosmogenic exposure dating based on an analysis of compiled boulder exposure ages. Earth Planet. Sci. Lett. 302, 71–80.
Heyman, J., Applegate, P.J., Blomdin, R., Gribenski, N., Harbor, J.M., Stroeven, A.P., 2016. Boulder height - exposure age relationships from a global glacial 10Be compilation. Quat. Geochronol. 34, 1–11.
Hippe, K., Ivy-Ochs, S., Kober, F., Zasadni, J., Wieler, R., Wacker, L., Kubik, P.W., Schlüchter, C., 2014. Chronology of Lateglacial ice flow reorganization and deglaciation in the Gotthard Pass area, Central Swiss Alps, based on cosmogenic 10Be and in situ 14C. Quat. Geochronol. 19, 14–26.
Hofmann, F., 1967. Geologischer Atlas der Schweiz 1: 25 000 Blatt 1052 Andelfingen. Kümmerly & Frey AG, Bern.
Hofmann, F., 1973. Geologischer Atlas der Schweiz 1: 25 000 Blatt 1074 Bischofszell. Schweizerische Geologische Kommission, Basel.
Hofmann, F., 1981. Geologischer Atlas der Schweiz 1: 25 000 Blatt: 1031 Neunkirch. Schweizerische Geologische Kommission, Basel.
Hofmann, F., 1993. Geologischer Atlas der Schweiz 1: 25 000 Blatt: 1073 Wil. Landeshydrologie und -geologie, Bern.
Hofmann, F., 1997. Blatt 1011 Beggingen (Südhälfte) mit SW-Anteil von Blatt 1012 Singen - Geol. Atlas Schweiz 1: 25 000, Karte 97. Bundesamt für Wasser und Geologie, Bern.
Hottinger, L., Matter, A., Nabholz, W., Schindler, C., 1970. Geologischer Atlas der Schweiz 1: 25 000 Blatt: 1093 Hörnli. Kümmerly & Frey AG, Bern.
Hübscher, J., 1961. Geologischer Atlas der Schweiz 1: 25 000 Blatt 1032 Diessenhofen Mit Anhängsel von Blatt 1031 Neunkirch. Wassermann AG, Basel.
Hug, J., 1917. Die letzte Eiszeit der Umgebung von Zürich. In: Festschrift der Naturforschenden Gesellschaft in Zürich. Beer, Zurich, pp. 125–143.
Ibele, T., Bissig, P., Allemann, F., 2016. Blatt 1135 Buchs. – Geol. Atlas Schweiz 1: 25 000, Karte 149. Bundesamt für Landestopografie swisstopo, Wabern.
Imhof, M.A., Cohen, D., Seguinot, J., Aschwanden, A., Funk, M., Jouvet, G., 2019. Modelling a paleo valley glacier network using a hybrid model: an assessment with a Stokes ice flow model. J. Glaciol. 65, 1000–1010.
Ivy-Ochs, S., 1996. The dating of rock surfaces using in situ produced 10Be, 26Al and 36Cl, with examples from Antarctica and the Swiss Alps. ETH, Zürich. MSc thesis.
Ivy-Ochs, S., Schäfer, J., Kubik, P.W., Synal, H.A., Schlüchter, C., 2004a. Timing of deglaciation on the northern Alpine foreland (Switzerland). Eclogae Geol. Helv. 97, 47–55.
Ivy-Ochs, S., Synal, H.-A., Roth, C., Schaller, M., 2004b. Initial results from isotope dilution for Cl and 36Cl measurements at the PSI/ETH Zurich AMS facility. Nucl. Instrum. Methods Phys. Res. B: Beam Interact. Mater. At. 223–224, 623–627.
Ivy-Ochs, S., Kober, F., 2008. Surface exposure dating with cosmogenic nuclides. Quat. Sci. J. 57, 179–209.
Ivy-Ochs, S., Kerschner, H., Maisch, M., Christl, M., Kubik, P.W., Schlüchter, C., 2009. Latest Pleistocene and Holocene glacier variations in the European Alps. Quat. Sci. Rev. 28, 2137–2149.
Ivy-Ochs, S., Lucchesi, S., Baggio, P., Fioraso, G., Gianotti, F., Monegato, G., Graf, A., Akçar, N., Christl, M., Carraro, F., Forno, M.G., Schlüchter, C., 2018. New geomorphological and chronological constraints for glacial deposits in the Rivoli-Avigliana end-moraine system and the lower Susa Valley (Western Alps, NW Italy). J. Quat. Sci. 33, 550–562.
Ivy-Ochs, S., Monegato, G., Reitner, J.M., 2022. The Alps: glacial landforms from the Last Glacial Maximum. In: Palacios, D., Hughes, P.D., Ruiz, J.M.G., de Andrés, N. (Eds.), European Glacial Landscapes: Maximum Extent of Glaciations. Elsevier, Amsterdam, pp. 449–460.
Jäckli, H., 1962. Die Vergletscherung der Schweiz im Würmmaximum. Eclogae Geol. Helv. 55, 285–294.
Jäckli, H., 1966. Geologischer Atlas der Schweiz 1: 25 000 Blatt: 1090 Wohlen. Orell Füssli, Zürich.
Jäckli, H., Hantke, R., Imhof, E., Leuzinger, H., 1970. Die Schweiz Zur Letzten Eiszeit = La Suisse Durant la dernière période Glaciaire = La Svizzera Durante l'ultima Glaciazione, Atlas der Schweiz 6. Eidg, Landestopographie, Wabern.
Jones, R.S., Small, D., Cahill, N., Bentley, M.J., Whitehouse, P.L., 2019. iceTEA: Tools for plotting and analysing cosmogenic-nuclide surface-exposure data from former ice margins. Quat. Geochronol. 51, 72–86.
Jordan, P., 2010. Analysis of overdeepened valleys using the digital elevation model of the bedrock surface of Northern Switzerland. Swiss J. Geosci. 103, 375–384.
Jordan, P., Eberhard, M., Graf, H.R., Diebold, P., Jost, J., Schürch, R., 2011. Blatt 1089 Aarau. - Geol. Atlas Schweiz 1: 25 000, Karte 135. Bundesamt für Landestopografie swisstopo, Wabern.
Kamleitner, S., Ivy-Ochs, S., Monegato, G., Gianotti, F., Akçar, N., Vockenhuber, C., Christl, M., Synal, H., 2022. The Ticino-Toce glacier system (Swiss-Italian Alps) in the framework of the Alpine last Glacial Maximum. Quat. Sci. Rev. 279, 107400.
Keller, F., 1846a. Allgemeine Bemerkungen über die Heidengräber in der Schweiz. Mitteilungen der Antiq. Gesellschaft Zürich 3, 55–101.
Keller, F., 1846. Beschreibung der helvetischen Heidengräber und Todtenhügel, welche seit dem Jahre 1836 eröffnet worden. In: Mitteilungen der Antiquarischen Gesellschaft in Zürich Band 3, Abtheilung 2, Heft 2 3, pp. 9–54.
Keller, O., 2021. The landscape of the Rhine Glacier in the Lake Constance Area. In: Reynard, E. (Ed.), Landscapes and Landforms of Switzerland. World Geomorphological Landscapes, Springer, Cham, pp. 289–304.
Keller, O., Krayss, E., 1987. Die hochwürmzeitlichen Rückzugsphasen des Rhein-Vorlandgletschers und der erste alpine Eisrandkomplex im Spätglazial. Geogr. Helv. 2, 169–178.
Keller, O., Krayss, E., 1993. The Rhine-Linth glacier in the Upper Wurm: a model of the last alpine glaciation. Quat. Int. 18, 15–27.
Keller, O., Krayss, E., 2000. Die Hydrographie des Bodenseeraums in Vergangenheit und Gegenwart. Berichte der St. Gall. Naturwissenschaftlichen Gesellschaft 89, 39–56.
Keller, O., Krayss, E., 2005a. Der Rhein-Linth-Gletscher im letzten Hochglazial. 2. Teil: Datierung und Modelle der Rhein-Linth-Vergletscherung. In: Klima-

Rekonstruktionen. Vierteljahrsschrift der Naturforschenden Gesellschaft Zürich, 150, pp. 69–85.
Keller, O., Krayss, E., 2005b. Der Rhein-Linth-Gletscher im letzten Hochglazial. 1. Teil: Einleitung; Aufbau und Abschmelzen des Rhein-Linth-Gletschers im Oberen Würm. In: Vierteljahrsschrift der Naturforschenden Gesellschaft Zürich, 150, pp. 19–32.
Kelly, M.A., Ivy-Ochs, S., Kubik, P.W., von Blanckenburg, F., Schlüchter, C., 2006. Chronology of deglaciation based on 10Be dates of glacial erosional features in the Grimsel Pass region, central Swiss Alps. Boreas 35, 634–643.
Klasen, N., Fiebig, M., Preusser, F., Reitner, J.M., Radtke, U., 2007. Luminescence dating of proglacial sediments from the Eastern Alps. Quat. Int. 164–165, 21–32.
Kohl, C.P., Nishiizumi, K., 1992. Chemical isolation of quartz for measurement of in-situ-produced cosmogenic nuclides. Geochim. Cosmochim. Acta 56, 3583–3587.
Kronig, O., Ivy-Ochs, S., Hajdas, I., Christl, M., Wirsig, C., Schlüchter, C., 2018. Holocene evolution of the Triftje- and the Oberseegletscher (Swiss Alps) constrained with 10Be exposure and radiocarbon dating. Swiss J. Geosci. 111, 117–131.
Krüger, T., 2013. Discovering the Ice Ages: International Reception and Consequences for a Historical Understanding of Climate. Brill, Leiden.
Labhart, T., 2013. Steinindustrie. Hist. Lex. der Schweiz (HLS), Version vom 10.01.2013. Online. https//hls-dhs-dss.ch/de/articles/014015/2013-01-10/. (Accessed 29 December 2021).
Lal, D., 1991. Cosmic ray labeling of erosion surfaces: in situ nuclide production rates and erosion models. Earth Planet. Sci. Lett. 104, 424–439.
Löpfe, R., Ibele, T., Wohlwend, S., Lüthold, A., Broggi, R., Allemann, F., 2018. Blatt 1155 Sargans. - Geol. Atlas Schweiz 1: 25 000, Karte 157. Bundesamt für Landestopografie swisstopo, Wabern.
Lotter, A., 1988. Paläoökologische und paläolimnologische Studie des Rotsees bei Luzern. Pollen-, grossrest-, diatomeen- und sedimentanalytische Untersuchungen. Diss. Bot. 124, 187.
Ludwig, A., 1930. Geologischer Atlas der Schweiz 1: 25 000 Blätter 218 Flawil 219 Herisau 220 Brunnadern 221 Schwellbrunn. A. Francke A.G, Bern.
Luetscher, M., Boch, R., Sodemann, H., Spötl, C., Cheng, H., Edwards, R.L., Frisia, S., Hof, F., Müller, W., 2015. North Atlantic storm track changes during the last Glacial Maximum recorded by Alpine speleothems. Nat. Commun. 6, 27–32.
Marrero, S.M., Phillips, F.M., Caffee, M.W., Gosse, J.C., 2016. CRONUS-Earth cosmogenic 36Cl calibration. Quat. Geochronol. 31, 199–219.
Moegle, V.E., 1994. Supermaximalphasen des würmhochglazialen Rhein-Vorland-Gletschers Beobachtungen bei lngoldingen (Kreis Biberach/Riß, Baden-Württ.). In: Jber. Mitt. oberrhein. geol. Ver., N.F. 76, pp. 335–350.
Monegato, G., Ravazzi, C., Donegana, M., Pini, R., Calderoni, G., Wick, L., 2007. Evidence of a two-fold glacial advance during the last glacial maximum in the Tagliamento end moraine system (Eastern Alps). Quat. Res. 68, 284–302.
Monegato, G., Scardia, G., Hajdas, I., Rizzini, F., Piccin, A., 2017. The Alpine LGM in the boreal ice-sheets game. Sci. Rep. 7, 1–8.
Mühlberg, F., 1905. Erläuterungen zur geologischen Karte des unteren Aare-, Reuss- und Limmat-Tales in 1: 25 000. In: Geologische Spezialkarten der Schweiz Nr. 31. Geologische Kommission der Schweizer Naturforschenden Gesellschaft, Bern.
Pavoni, N., Jäckli, H., Schindler, C., 1992. Blatt 1091 Zürich. - Geol. Atlas Schweiz 1: 25 000, Karte 90. Bundesamt für Landestopografie swisstopo, Wabern.
Pawełczyk, F., Hajdas, I., Sadykov, T., Blochin, J., Caspari, G., 2022. Comparing analysis of pretreatment methods of wood and bone materials for the chronology of peripheral burials at Tunnug 1, Tuva Republic, Russia. Radiocarbon 64, 171–186.
Penck, A., Brückner, E., 1909. Die Alpen Im Eiszeitalter. Chr. Herm. Tauchnitz, Leipzig.
Pietsch, J., Jordan, P., 2014. Arbeitsbericht NAB 14-02. Digitales Höhenmodell Basis Quartär der Nordschweiz – Version 2014 und ausgewählte Auswertungen. Nagra, Wettingen.
Preusser, F., Blei, A., Graf, H., Schlüchter, C., 2007. Luminescence dating of Würmian (Weichselian) proglacial sediments from Switzerland: methodological aspects and stratigraphical conclusions. Boreas 36, 130–142.
Preusser, F., Graf, H.R., Keller, O., Krayss, E., Schlüchter, C., 2011. Quaternary glaciation history of northern Switzerland. E&G Quat. Sci. J. 60, 282–305.
Putkonen, J., Swanson, T., 2003. Accuracy of cosmogenic ages for moraines. Quat. Res. 59, 255–261.
Quarta, G., Molnár, M., Hajdas, I., Calcagnile, L., Major, I., Jull, A.J.T., 2021. 14C Intercomparison exercise on bones and ivory samples: implications for forensics. Radiocarbon 63, 533–544.
Ravazzi, C., Badino, F., Marsetti, D., Patera, G., Reimer, P.J., 2012. Glacial to paraglacial history and forest recovery in the Oglio glacier system (Italian Alps) between 26 and 15 ka cal BP. Quat. Sci. Rev. 58, 146–161.
Ravazzi, C., Pini, R., Badino, F., De Amicis, M., Londeix, L., Reimer, P.J., 2014. The latest LGM culmination of the Garda Glacier (Italian Alps) and the onset of glacial termination. Age of glacial collapse and vegetation chronosequence. Quat. Sci. Rev. 105, 26–47.
Reber, R., Akçar, N., Ivy-Ochs, S., Tikhomirov, D., Burkhalter, R., Zahno, C., Lüthold, A., Kubik, P.W., Vockenhuber, C., Schlüchter, C., 2014. Timing of retreat of the Reuss Glacier (Switzerland) at the end of the last Glacial Maximum. Swiss J. Geosci. 107, 293–307.
Regierungspräsidium Freiburg Landesamt für Geologie, Rohstoffe und Bergbau (Ed.), 2013. Geologische Karte 1 : 50 000, Geodaten der Integrierten Geowissenschaftlichen Landesaufnahme (GeoLa).
Reimer, P.J., Austin, W.E.N., Bard, E., Bayliss, A., Blackwell, P.G., Bronk Ramsey, C., Butzin, M., Cheng, H., Edwards, R.L., Friedrich, M., Grootes, P.M., Guilderson, T.P., Hajdas, I., Heaton, T.J., Hogg, A.G., Hughen, K.A., Kromer, B., Manning, S.W., Muscheler, R., Palmer, J.G., Pearson, C., van der Plicht, J., Reimer, R.W., Richards, D.A., Scott, E.M., Southon, J.R., Turney, C.S.M., Wacker, L., Adolphi, F., Büntgen, U., Capano, M., Fahrni, S.M., Fogtmann-Schulz, A., Friedrich, R., Köhler, P., Kudsk, S., Miyake, F., Olsen, J., Reinig, F., Sakamoto, M., Sookdeo, A., Talamo, S., 2020. The IntCal20 Northern Hemisphere Radiocarbon Age Calibration Curve (0–55 cal kBP). Radiocarbon 62, 725–757.
Reitner, J.M., 2007. Glacial dynamics at the beginning of termination I in the Eastern Alps and their stratigraphic implications. Quat. Int. 164–165, 64–84.
Rey, F., Gobet, E., Schwörer, C., Hafner, A., Szidat, S., Tinner, W., 2020. Climate impacts on vegetation and fire dynamics since the last deglaciation at Moossee (Switzerland). Clim. Past 16, 1347–1367.
Rey, R., Wildberger, A., Frank, S., Freimoser, M., 2011. Blatt 1072 Winterthur. – Geol. Atlas Schweiz 1: 25 000 Karte 140. Bundesamt für Landestopografie swisstopo, Wabern.
Ribolini, A., Spagnolo, M., Cyr, A.J., Federici, P.R., 2022. Last Glacial Maximum and early deglaciation in the Stura Valley, southwestern European Alps. Quat. Sci. Rev. 295, 107770.
Roattino, T., Crouzet, C., Vassallo, R., Buoncristiani, J.-F., Carcaillet, J., Gribenski, N., Valla, P.G., 2022. Paleogeographical reconstruction of the western French Alps foreland during the last glacial maximum using cosmogenic exposure dating. Quat. Res. 1–16.
Samartin, S., Heiri, O., Vescovi, E., Brooks, S.J., Tinner, W., 2012. Lateglacial and early Holocene summer temperatures in the southern Swiss Alps reconstructed using fossil chironomids. J. Quat. Sci. 27, 279–289.
Saxer, F., 1965. Geologischer Atlas der Schweiz 1: 25 000 Blatt: 1075 Rorschach. Kümmerly & Frey AG, Bern.
Scapozza, C., Castelletti, C., Soma, L., Dall'Agnolo, S., Ambrosi, C., 2014. Timing of LGM and deglaciation in the Southern Swiss Alps. Geomorphol. Reli. Process. Environ. 4, 307–322.
Schälli, L., 2012. TheDiffluence of the Rhine Glacier at Sargans in Connection to the Solid - RockSurface Model of the Rhine and Seez Valley. University of Zurich, Zurich. MSc thesis.
Schimper, K.F., 1837. Auszug aus dem Briefe des H. Dr Schimper: über die Eiszeit. Actes la Société Helvétique des Sci. Na-turelles 22, 38–51.
Schindler, C., Röthlisberger, H., Gyger, M., 1978. Glaziale Stauchungen in den Niederterrassen-Schotter des Aadorfer Feldes und ihre Deutung. Eclogae Geol. Helv. 71, 159–174.
Schlüchter, C., 1988. The deglaciation of the Swiss-Alps: a paleoclimatic event with chronological problems. Bull. l'Association française pour l'étude du Quat. 25, 141–145.
Schlüchter, C., Akçar, N., Ivy-Ochs, S., 2021. The Quaternary period in Switzerland. In: Reynard, E. (Ed.), Landscapes and Landforms of Switzerland. World Geomorphological Landscapes, Springer, Cham, pp. 47–69.
Schmidle, W., 1914. Die diluviale Geologie der Bodenseegegend. In: Die Rheinlande in naturwissenschaftlichen und geographischen Einzeldarstellungen Nr. 8. Westermann, Braunschweig.
Schmidt, M., 1911. Rückzugstadien der Würmvergletscherung im Argengebiet. In: Schriften des Vereines für Geschichte des Bodensees u. seiner Umgebung, pp. 26–53.
Schmidt, M., 1976. Erläuterungen zu Blatt 8223 Ravensburg. In: Geologische Karte von Baden-Württemberg 1:25000. Geologisches Landesamt Baden-Württemberg, Stuttgart.
Schreiner, A., 1968. Eiszeitliche Rinnen und Becken und deren Füllung im Hegau und westlichen Bodenseegebiet. Jahreshefte des Geol. Landesamts Baden-württemb. 10, 79–104.
Schreiner, A., 1973. Geologische Karte von Baden-Württemberg 1: 25 000. Erläuterungen zu Blatt 8219 Singen. Geologisches Landesamt Baden-Württemberg, Freiburg im Breisgau.
Schreiner, A., 1992. <book-title>Erläuterungen zu Blatt Hegau und westlicher Bodensee – 3. Aufl., Geologische Karte 1 </book-title>: 50 000 von Baden-Württemberg. Geologisches Landesamt Baden-Württemberg, Freiburg i. Br., Stuttgart.
Schreiner, A., 1992b. Einführung in Die Quartärgeologie. E. Schweizerbart'sche, Stuttgart.
Seguinot, J., Ivy-Ochs, S., Jouvet, G., Huss, M., Funk, M., Preusser, F., 2018. Modelling last glacial cycle ice dynamics in the Alps. Cryosphere 12, 3265–3285.
Serra, E., Valla, P.G., Gribenski, N., Carcaillet, J., Deline, P., 2022. Post-LGM glacial and geomorphic evolution of the Dora Baltea valley (western Italian Alps). Quat. Sci. Rev. 282, 107446.
Spötl, C., Reimer, P.J., Göhlich, U.B., 2018. Mammoths inside the Alps during the last glacial period: Radiocarbon constraints from Austria and palaeoenvironmental implications. Quat. Sci. Rev. 190, 11–19.
Spötl, C., Koltai, G., Jarosch, A.H., Cheng, H., 2021. Increased autumn and winter precipitation during the Last Glacial Maximum in the European Alps. Nat. Commun. 12, 1839.
Starnberger, R., Rodnight, H., Spötl, C., 2011. Chronology of the last Glacial Maximum in the Salzach palaeoglacier area (Eastern Alps). J. Quat. Sci. 26, 502–510.
Stone, J.O., 2000. Air pressure and cosmogenic isotope production. J. Geophys. Res. Solid Earth 105, 23753–23759.
Stone, J.O., Allan, G.L., Fifield, L.K., Cresswell, R.G., 1996. Cosmogenic chlorine-36 from calcium spallation. Geochim. Cosmochim. Acta 60, 679–692.
Stone, J.O., Evans, J.M., Fifield, L.K., Allan, G.L., Cresswell, R.G., 1998. Cosmogenic chlorine-36 production in calcite by muons. Geochim. Cosmochim. Acta 62, 433–454.
Stone, J.O., Fifield, K., Vasconcelos, P., 2005. Terrestrial chlorine-36 production from spallation of iron. In: Abstr. 10th Int. Conf. Accel. Mass Spectrom.
Stuiver, M., Polach, H.A., 1977. Discussion: reporting of 14 C data. Radiocarbon 19, 355–363.
Synal, H.A., Bonani, G., Döbeli, M., Ender, R.M., Gartenmann, P., Kubik, P.W., Schnabel, C., Suter, M., 1997. Status report of the PSI/ETH AMS facility. Nucl. Instruments Methods Phys. Res. SectB Beam Interact. with Mater. Atoms 123, 62–68.

Synal, H.A., Stocker, M., Suter, M., 2007. MICADAS: a new compact radiocarbon AMS system. Nucl. Instruments Methods Phys. Res. SectB Beam Interact. with Mater. Atoms 259, 7–13.
van Husen, D., 1987. Die Ostalpen und ihr Vorland in der letzten Eiszeit (Würm). Geologische Bundesanstalt, Wien.
van Husen, D., 1997. LGM and late-glacial fluctuations in the Eastern Alps. Quat. Int. 38–39, 109–118.
van Klinken, G.J., 1999. Bone collagen quality indicators for palaeodietary and radiocarbon measurements. J. Archaeol. Sci. 26, 687–695.
Velasquez, P., Messmer, M., Raible, C.C., 2020. A new bias-correction method for precipitation over complex terrain suitable for different climate states: a case study using WRF (version 3.8.1). Geosci. Model Dev. 13, 5007–5027.
Velasquez, P., Kaplan, J.O., Messmer, M., Ludwig, P., Raible, C.C., 2021. The role of land cover in the climate of glacial Europe. Clim. Past 17, 1161–1180.
Velasquez, P., Messmer, M., Raible, C.C., 2022. The role of ice-sheet topography in the Alpine hydro-climate at glacial times. Clim. Past 18, 1579–1600.
Venetz, I., 1830. Sur l'ancienne extension des glaciers et sur leur retraite dans leur limites actuelles. Actes la Société Helvétique des Sci. Nat. Quinzième Réunion Annuelle à l'Hospice du Grand-Saint-bernard les 21, 22 et 23 juillet 1829, 15, 31.
Višnjević, V., Herman, F., Prasicek, G., 2020. Climatic patterns over the European Alps during the LGM derived from inversion of the paleo-ice extent. Earth Planet. Sci. Lett. 538, 116185.
Vockenhuber, C., Miltenberger, K.U., Synal, H.A., 2019. 36Cl measurements with a gas-filled magnet at 6 MV. Nucl. Instruments Methods Phys. Res. SectB Beam Interact. with Mater. Atoms 455, 190–194.
Wacker, L., Němec, M., Bourquin, J., 2010. A revolutionary graphitisation system: fully automated, compact and simple. Nucl. Instruments Methods Phys. Res. SectB Beam Interact. with Mater. Atoms 268, 931–934.
Weidenbach, F., 1975. Geologische Karte von Baden-Württemberg 1: 25000. Blatt 8023 Aulendorf. Geologisches Landesamt Baden-Württemberg, Freiburg im Breisgau.
Wirsig, C., Zasadni, J., Christl, M., Akçar, N., Ivy-Ochs, S., 2016. Dating the onset of LGM ice surface lowering in the High Alps. Quat. Sci. Rev. 143, 37–50.
Wüthrich, L., Morabito, E.G., Zech, J., Trauerstein, M., Veit, H., Gnägi, C., Merchel, S., Scharf, A., Rugel, G., Christl, M., Zech, R., 2018. 10Be surface exposure dating of the last deglaciation in the Aare Valley. Switzerland. Swiss J. Geosci. 111, 295–303.
Wyssling, G., 2007. Blatt 1092 Uster. – Geol. Atlas Schweiz 1: 25 000, Karte 128. Bundesamt für Landestopografie swisstopo, Wabern.
Zaugg, A., 2007. Blatt 1055 Romanshorn. – Geol. Atlas Schweiz 1: 25 000, Karte 125. Bundesamt für Landestopografie swisstopo, Wabern.
Zaugg, A., Geyer, M., 2008. Blatt 1033/1034 Steckborn-Kreuzlingen. – Geol. Atlas Schweiz 1: 25 000, Karte 112. Bundesamt für Landestopografie swisstopo, Wabern.
Zbinden, H., Andree, M., Oeschger, H., Ammann, B., Lotter, A., Bonani, G., Wölfli, W., 1989. Atmospheric radiocarbon at the end of the last Glacial: an estimate based on AMS radiocarbon dates on terrestrial macrofossils from Lake Sediments. Radiocarbon 31, 795–804.